

Microscale imaging of cilia-driven fluid flow

Brendan K. Huang · Michael A. Choma

Received: 8 September 2014/Revised: 12 November 2014/Accepted: 13 November 2014/Published online: 23 November 2014
© Springer Basel 2014

Abstract Cilia-driven fluid flow is important for multiple processes in the body, including respiratory mucus clearance, gamete transport in the oviduct, right–left patterning in the embryonic node, and cerebrospinal fluid circulation. Multiple imaging techniques have been applied toward quantifying ciliary flow. Here, we review common velocimetry methods of quantifying fluid flow. We then discuss four important optical modalities, including light microscopy, epifluorescence, confocal microscopy, and optical coherence tomography, that have been used to investigate cilia-driven flow.

Keywords Microfluidic flow · Mucus · Velocimetry · Particle tracking · Digital particle image velocimetry · Confocal microscopy · Fluorescence microscopy · Optical coherence tomography

An overview of ciliary physiology

Motile cilia drive fluid flow in multiple organ systems

Cilia are hair-like organelles projecting from specialized epithelial surfaces of the body. *Motile cilia* are responsible for generating microfluidic flow in a variety of organ systems (Fig. 1), and defects in cilia-driven fluid flow can have severe disease manifestations. In the lung, bacteria and particulate matter are removed by *mucociliary clearance*, the process whereby mucus, a biochemical barrier to pathogens, is transported by motile cilia out of the respiratory tract [1]. Defects in mucociliary clearance can result in recurrent pulmonary infections in diseases such as cystic fibrosis [2] and primary ciliary dyskinesia (PCD) [3]. In the oviduct, cilia drive the transport of ova [4], and defects in cilia such as in PCD can lead to infertility. A transient organ during embryonic development known as the embryonic node also contains cilia and is responsible for determining right–left asymmetry [5]. Patients with PCD and hence impaired nodal flow can exhibit situs inversus, a condition in which organs are located in the mirror position in the body. Finally, the ventricles of the brain are lined with cilia that contribute to the circulation of cerebrospinal fluid (CSF) [6]. Intriguingly, an accumulation of CSF known as hydrocephalus also is associated with PCD [7].

Given the numerous sites where cilia play a critical role in the body as well as the severe disease manifestations that occur when cilia are defective, there is much interest from both clinicians and basic scientists in imaging cilia-driven fluid flow. Although cilia were described as early as 1671 by Leeuwenhoek [8], because of the complexity of studying ciliary physiology, there continues to be active research in techniques for ciliary imaging. One reason why studying cilia can be challenging arises from the fact that ciliary

B. K. Huang (✉) · M. A. Choma
Department of Biomedical Engineering, Yale University,
New Haven, USA
e-mail: brendan.huang@yale.edu

M. A. Choma
Department of Diagnostic Radiology, Yale School of Medicine,
New Haven, USA

M. A. Choma
Department of Pediatrics, Yale School of Medicine,
New Haven, USA

M. A. Choma
Department of Applied Physics, Yale University,
New Haven, USA

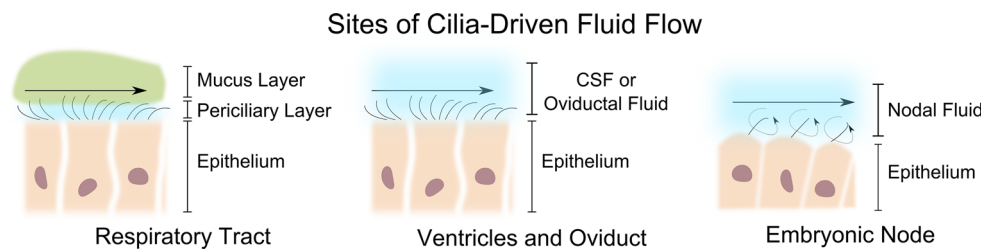


Fig. 1 Anatomic sites of ciliary action. Cilia are found in several organ systems, including (*left*) the respiratory and nasal tract, where the airway surface liquid is divided into the periciliary layer and the mucus layer, (*middle*) the ventricles of the brain and the oviduct,

where no such layered structure exists, and (*right*) the transient embryonic node, in which ciliary-driven flow is thought to be generated by rotating cilia

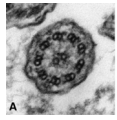
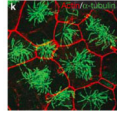
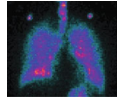
action takes place over a large range of length scales, and any single imaging technique can only probe a portion of those length scales. Thus, no single modality tells a complete story. Another reason is that current-generation technologies are not sufficiently fast to capture two important dynamic processes: the three-dimensional motion of individual cilia, and the three-dimensional, three-vector component cilia-driven flow field.

In this review, we will first give an overview of the multiple scales of ciliary physiology. We will then discuss velocimetry as a general matter and describe common physical methods of interrogating fluid flow, including image and point-based techniques. We will lastly review the main optical modalities for imaging ciliary flow, including historically important methods (light microscopy), the current standards, (epifluorescence and confocal fluorescence microscopy), and promising emerging methods (optical coherence tomography).

Cilia exert their effects over multiple length scales

On the smallest, nanoscopic scale, motile cilia are made up of microtubules, each about 25 nm wide [9]. These microtubules are arranged either in a “9 + 2” pattern (Fig. 2, *top*) in most sites [10] or a “9 + 0” pattern at the node [11]. ATP-powered molecular motor proteins known as dyneins are attached to the microtubules [12]. According to the sliding filament model of ciliary motion, dynein motors walk along microtubular filaments, while pulling on adjacent filaments to cause the cilium to beat [13]. To study ciliary structure at this nanoscopic scale, transmission electron microscopy (TEM) has the requisite resolution to see features such as dynein arms and microtubular structure. Sample fixation, however, is necessary for TEM preparation and thus precludes study of the dynamics of functioning cilia [14].

On a slightly larger size scale, an individual cilium extends on the order of $\sim 10 \mu\text{m}$ in length [15]. Each cilium beats at a given tempo, known as the ciliary beat frequency (CBF) [16]. Because measuring CBF does not

Size Scale	Imaging Modality
10 nm ultrastructure	TEM 
10 μm microfluidic flow	Brightfield Epifluorescence Confocal OCT 
10 cm anatomic clearance	CT Radiotracer 

Length Scales of Ciliary Action

Fig. 2 Ciliary physiology spans many length scales, requiring multiple imaging modalities (*top*). Ciliary ultrastructure such as microtubules and motor proteins can be imaged by transmission electron microscopy (TEM) (image reproduced from [3]) (*middle*). Microfluidic flow can be imaged by optical modalities such as light microscopy, epifluorescence, confocal, and optical coherence tomography (OCT). The image here shows cilia in the ventricle as visualized by confocal fluorescence (image reproduced from [157]) (*bottom*). Anatomic clearance of mucus can be quantified by radiotracer methods (image reproduced from [187]) and computed X-ray tomography (CT)

require resolving ultrastructure, but rather probing movement of the ciliary stalk, CBF can be measured by techniques with less stringent resolution requirements. The most common modalities for measuring CBF include (1) light scattering, focusing light on a small area of a ciliated surface and analyzing the frequency content of a back-scattered signal on a photodiode [16], and (2) using white light or differential interference contrast (DIC) microscopy combined with high-speed video imaging to resolve actual cilia themselves [17, 18]. Other forms of microscopy such as confocal fluorescence microscopy to directly visualize cilia have also been applied [19, 20].

On yet a larger length scale of approximately 10–100 μm , many cilia line a surface (Fig. 2, *middle*).

There may be 200 cilia on a given epithelial cell, and many cells adjacent to each other [13]. These adjacent cilia need to beat in the same direction to drive flow [21], and they may also beat in coordinated, metachronal waves to properly propel fluid [15]. In addition, in the respiratory tract specifically, the cilia themselves are situated in the airway surface liquid (ASL), the fluid that covers the epithelial lining of conductive airways (Fig. 1, left). The ASL in turn is composed of the periciliary layer (PCL), an approximately 7- μm -thick fluid layer where the cilia themselves reside [22], and the mucus layer (ML), the viscoelastic mucus material that sits directly above the periciliary layer [23]. The mucus layer can vary considerably in thickness and has been measured to be anywhere from 8 to 200 μm [24]. At these length scales, flow is characterized by a low Reynolds number and is often denoted as microfluidic flow [25, 26]. For the purposes of this article, we denote the intermediate, microscopic scale over which cilia generate flow as microfluidic cilia-driven fluid flow, and the investigation of fluid flow at this scale will be the subject of this review article.

The largest length scale of ciliary action is the anatomic scale of multiple centimeters. Microfluidic flows must coalesce to create bulk transport of mucus through the conductive airways of the lungs, which range in size from sub 1-mm-diameter bronchioles to the $\sim 2\text{-cm}$ -diameter trachea [1, 27], or through the oviduct, for example, which can be $\sim 10\text{ cm}$ long [28]. Although flow is still low Reynolds number, given the larger size scale of movement, we refer to this anatomic clearance of fluid (Fig. 2, bottom) as macroscopic flow. Clearance on this macroscopic scale is most often investigated through radioactive methods, e.g., by having a patient inhale radioactively labeled colloids and imaging movement with a gamma camera [14]. Other methods, such as timing transit time of saccharin in the nasal sinuses [29], fluoroscopic methods [30], or using real-time CT to track tantalum discs [31, 32] can also be used to assay anatomic clearance.

Optical techniques are well suited for microfluidic imaging

To image microfluidic cilia-driven flow, then, we require techniques with 1–10 μm spatial resolution but that can also image over a relatively large field of view of at least 1 mm. In addition, the techniques should be non-destructive to cells and tissue as not to perturb functional dynamics. Optical microscopy satisfies these criteria and is well suited toward studying cilia-driven flow at the microfluidic scale.

As shown in Fig. 3, when imaging cilia-driven fluid flow, there are three main choices to make. First, one must choose which ciliary system to investigate. Second, one

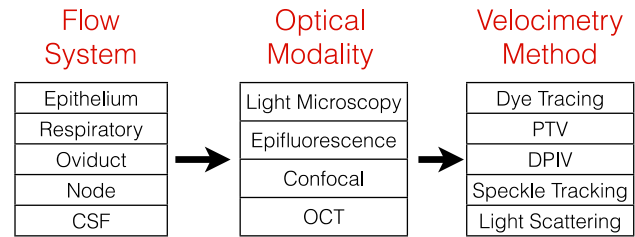


Fig. 3 Workflow of ciliary imaging. For any given choice of flow system (left column) to be imaged, an optical imaging modality can be chosen (middle column) and combined with a choice of velocimetry technique (right column). Typically, the imaging modality will determine contrast and cross-sectional ability, while the velocimetry technique will determine the extent of velocimetry information recovered. *CSF* cerebrospinal fluid. *OCT* optical coherence tomography. *PTV* particle tracking velocimetry. *DPIV* digital particle image velocimetry

must decide on the optimal optical imaging modality. And third, one must apply a specific velocimetry technique to that imaging modality. Each of these choices can be made relatively independently, and many combinations of flow system, modality, and velocimetry technique have been demonstrated in the literature. Given the many ways of imaging cilia-driven flow, familiarity with both the optical modalities, discussed in “Microscale imaging of cilia-driven fluid flow”, and the various velocimetry techniques, discussed in “Microfluidic velocimetry”, is crucial to selecting the proper approach for studying the ciliary physiology in question.

Microfluidic velocimetry

Velocimetry refers to the measurement of the velocity of objects. Because fluids may vary in their properties over space, one way of describing fluid velocity is by describing the fluid flow velocity field [33]. A fluid flow velocity field, often simply called a flow field, is a type of vector field that specifies the three-component velocity $\mathbf{v} = (v_x, v_y, v_z)$ of a fluid at every point in space $\mathbf{r} = (x, y, z)$ and time t [34]. An example of a flow field, generated by nodal cilia, is shown in Fig. 4. The velocity is a vector quantity specified by the magnitude of velocity or speed defined as $s = (v_x^2 + v_y^2 + v_z^2)^{1/2}$, as well as the direction of flow at a specific location $\mathbf{r} = (x, y, z)$. The velocity can often be approximated as stationary or steady state, in which case it does not vary in time [34]. In the context of this review, we assume that cilia-driven fluid velocities are steady state over the measurement period.

In measuring steady-state flow, then, one must measure six parameters to specify the flow velocity at a given point: three components of velocity, and three spatial coordinates. In addition to specifying velocity as a function of spatial

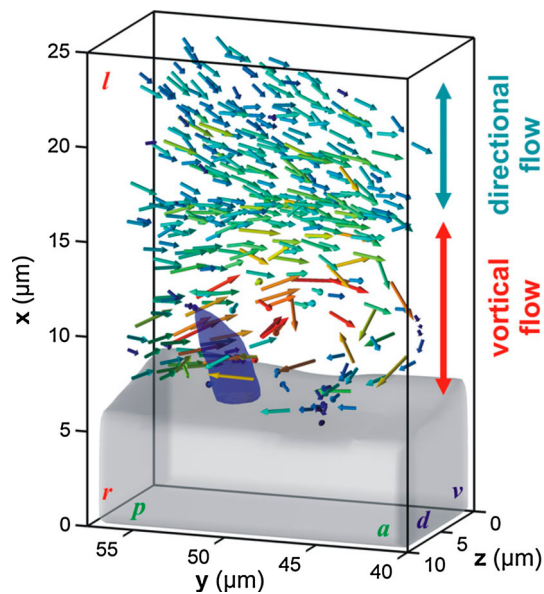


Fig. 4 Flow field generated by a single nodal cilium in a zebrafish embryo, reproduced from [169]. Here, the flow field specifies a magnitude (*color*) and direction of the velocity vector at every location in space, relative to epithelium (axes denoted as *d-v* dorsal ventral, *a-p* anterior posterior, and *l-r* left right). The flow field was estimated by employing three-dimensional, confocal fluorescent particle tracking velocimetry

location, the translational diffusivity of the particles, $D(x, y, z)$, or the rotational diffusivity $D_r(x, y, z)$ [25] can also be measured as a function of spatial location. Commonly, however, it may only be possible to measure the two-dimensional flow field, in which case the velocity $\mathbf{v} = (v_x, v_y)$ is specified at $\mathbf{r} = (x, y)$.

The goal of any implementation of microfluidic velocimetry is to measure velocity throughout a fluid. Velocimetry can be performed in many ways. Although these techniques are not necessarily neatly divisible into individual categories, we have found it useful to divide ciliary flow techniques based on two criteria. Experimenters will typically choose between (1) dye versus particle-based methods, and between using (2) image information (2D or 3D) to track features versus point-wise (0D), time-varying information to deduce velocity.

Dye-based approaches

Dye visualization

One straightforward method for visualizing flow is to inject dye into fluid and image its subsequent transport [35]. Visualization of dye movement is often enough to qualitatively differentiate the presence versus the absence of flow. In a slightly more sophisticated implementation, by recording a movie of the moving dye and calculating the

displacement of the dye over some period of time, one can also estimate a linear flow speed. Similarly, instead of imaging the dye, one can also use other chemical detection methods such as microdialysis probes located downstream of fluid flow to measure dye transport time over some distance. Grubb et al. [36] used this method to quantitatively estimate linear flow speed in the respiratory tract.

Molecular tagging velocimetry

Injecting dye has limitations, as it is not always possible to evenly seed the dye, and the needle itself may interfere with flow. One alternative strategy is to pre-mix a dye throughout the fluid and then use an optical pulse to activate, bleach, or otherwise modify the dye in a specific spatial region. This process is often called molecular tagging velocimetry [37, 38], and it has the advantage of being able to non-invasively generate a line of dye at a given instant. For instance, caged fluorophores can be released at a given location with a UV pulse, and the movement of the subsequent fluorescent dye can be traced to provide an estimate of velocity [37]. Although not as common, such approaches have been used to image mucociliary flow [22].

Experimental considerations of dye-based imaging

The main criterion for a dye is that it provides imaging contrast with the rest of the fluid. That is, based on the physical property being measured by the imaging modality, the dye must have some discernible signal that differs from the surrounding fluid [35]. In the case of simple color video microscopy, this contrast can be as simple as colored dye in a clear fluid. In the case of molecular tagging velocimetry, contrast can be given by other physical parameters such as fluorescence, bleaching, or absorptivity.

Another important consideration is that dye will simultaneously diffuse as it is transported. Diffusion leads to a root-mean-squared (RMS) displacement of $\Delta r^{\text{RMS}} = \langle \mathbf{r}(t)^2 \rangle^{1/2} = (2nD\Delta t)^{1/2}$, where n is the dimensionality of the measurement, D is the diffusivity, and Δt is the inter-frame time [39]. This RMS displacement can manifest itself as a source of noise in quantifying flow. Thus, the average displacement due to flow should be significantly larger than RMS movement due to dye diffusion [40].

Particle-based approaches

Another common approach to measure cilia-driven flow is to seed and track particles in the fluid. Many freely available programs exist to automatically implement particle tracking [41]. Particle-based approaches can be divided into three related techniques based upon the density of

particle seeding [42]. In the least dense case, known as particle tracking velocimetry (PTV), individual particles can be identified, localized, and matched from frame to frame. Increasing the density of particles to an intermediate regime makes particle matching less feasible, so instead subregions of an image are tracked in digital particle image velocimetry (DPIV). Finally, in the densest seeding where multiple particles occupy each focal volume in a laser-illuminated imaging system, speckle tracking is used to also track subregions of an image. In the two-dimensional implementations of these techniques, particles can undergo three types of motion: (1) in-plane translation, (2) out-of-plane translation orthogonal to the imaging plane, and (3) diffusion. As we will discuss, each of these types of motion will affect the particle-based techniques.

Particle tracking velocimetry

In particle tracking velocimetry (PTV), particles are first identified and then matched from frame to frame [42]. By following a particle from image to image and knowing the frame rate of the imaging device, one can estimate the velocity \mathbf{v} of each particle as $v_x(x, y, z) = \Delta x/\Delta t$, $v_y(x, y, z) = \Delta y/\Delta t$, and $v_z(x, y, z) = \Delta z/\Delta t$, where (x, y, z) is the vectorial position where the particle is tracked, $(\Delta x, \Delta y, \Delta z)$ is the displacement vector between two frames, and Δt is the interframe time. By tracking particles over an entire two-dimensional image, one can obtain a two-component velocity estimate as a function of two spatial locations, i.e., a two-dimensional flow field.

Two-dimensional PTV is the most common implementation of PTV, and two velocity components can be recovered. To gain three components of velocity, there are several strategies that can be employed [43], including using two perspectives (stereoscopic PIV) [44], using two planes of imaging (dual plane PIV) [45], or using holographic imaging to digitally refocus the image [46]. These implementations, which yield three-component velocity fields in two spatial dimensions, also require more complicated optical setups. Another way of recovering three components, now in three spatial dimensions, is to image sequential volumes. Many confocal microscopes, for example, are already equipped with volumetric imaging capabilities. Volumetric imaging, however, is typically much slower, and the limited imaging speed may limit the particle speed that can be tracked [47].

Experimental considerations of PTV

Similar to dyes selected for imaging, particles should provide sufficient imaging contrast with the fluid. Contrast in particles is typically achieved through color, light scattering, or fluorescence [48]. As with dye, beads also

undergo diffusion, which is manifest as an RMS displacement Δr^{RMS} in between each image frame. Diffusion, if unaccounted for in experimental design or data modeling, may limit velocimetry measurements but can also be measured separately (discussed below).

Another consideration of PTV is imaging speed. In two-dimensional PTV, in-plane motion is estimated as a particle is tracked. If a particle also has motion orthogonal to the imaging plane, it may transit through the imaging plane. The particle must be captured in at least two sequential frames to be tracked. Thus, the degree of out-of-plane motion should be estimated to determine the minimum imaging frame rate. In addition, if a particle is accelerating, either changing in speed or directionality as it moves, it can still be tracked. Between frames, however, the particle is assumed to undergo negligible acceleration.

Finally, one must ensure that particle movement is actually reflective of the velocity of the surrounding fluid. The difference in velocity of a particle with respect to the surrounding fluid is known as slip velocity [48]. For spherical particles, the slip velocity \mathbf{u}_s is given by $\mathbf{u}_s = d^2(\rho_p - \rho)\mathbf{a}_p/(18\mu)$. That is, the velocity difference between the fluid and particles is increased with larger particle radius d , particle acceleration \mathbf{a}_p , and differences in density between particle and fluid $(\rho_p - \rho)$, while it is decreased with greater viscosity μ . Thus, particles with low slip velocity should be chosen. Notably, the formula for slip velocity assumes that the molecules of the fluid are much smaller than the particle itself. This assumption may be violated in the case of mucus, which consists of large polymers that may approach the size of particles and may also have a complex nanotopology [49]. Moreover, mucus may be viscoelastic, having a component of frictional and restoring force, in which case more sophisticated models are required to interpret particle tracking data [50].

Measuring diffusivity with PTV

Once particles have been successfully tracked, PTV can additionally yield estimates of viscosity of the fluid. By tracking the Brownian motion of particles and specifically calculating the mean-squared displacement of particles, one can estimate the diffusivity $D = \langle \mathbf{r}(t)^2 \rangle / (2nT)$, where $\langle \mathbf{r}(t)^2 \rangle$ is the mean-squared displacement over some time interval T , and n is the dimensionality of measurement [50]. To convert these particle measurements into estimate of fluid parameters, the diffusivity D can be related to fluid viscosity by the Stokes–Einstein relationship [51]. Typically one must have an a priori measurement of particle diameter to estimate viscosity from Stokes–Einstein. Consequently, these measurements are usually performed with exogenously seeded particles, the properties of which are known in advance.

The diffusivity and velocity of a particle can be simultaneously estimated from particle tracking. In this case, the particle trajectory has an average drift, which gives its velocity, in addition to random displacements, which gives its diffusivity. The mean square displacement is then no longer linear with time, as it is in pure diffusion, but now also contains an additional quadratic term from velocity [50]. As mentioned previously in estimating velocity only, the particle is assumed not to undergo significant acceleration during the interrogation period. In estimating diffusivity and velocity simultaneously, however, the interrogation period is no longer the interframe time Δt , but a longer period T that lasts multiple frames.

Digital particle image velocimetry

In PTV, particles must be seeded sparsely to accurately match individual particles in adjacent frames. By definition, then, one recovers only a sparse number of velocity measurements in each frame. Increasing the particle density becomes problematic because particles cannot always be tracked with high fidelity. To increase the density of sampling, subregions of the image rather than individual particles are tracked in digital particle image velocimetry (DPIV) [52]. In such methods, the images are divided into subregions large enough to encompass features of the image, and these subregions from consecutive frames are compared against each other using spatial cross-correlation. When the maximum interframe cross-correlation is found, a feature is “tracked,” and a velocity \mathbf{v} can be assigned at a specific location (x, y, z) just as in particle tracking. This cross-correlation procedure then allows for mapping of flow fields even when exogenous particles cannot be applied or when the fluid has densely scattering particulate matter.

DPIV has many of the same characteristics as particle tracking. Like PTV, the number of velocity components is the same as the number of dimensions tracked unless specialized techniques are used [43]. In two-dimensional DPIV, in-plane translation of particles causes the same imaging feature to be translated in the image at a later time. Significant out-of-plane motion, as in PTV, may cause features to move through the imaging plane before they can be tracked. In addition, if particles are undergoing significant diffusive motion, the random motion with respect to one other may cause imaging features themselves to change, limiting the ability to track features accurately [53].

Speckle tracking

In the highest density of seeding, multiple particles occupy a single focal volume on average. If a laser or other spatially coherent light source (e.g., superluminescent diode) is used to illuminate the sample, then the image will exhibit a property

known as speckle. Speckle is a high-contrast intensity noise manifested as random-appearing patterns [54]. Like in DPIV, as particles undergo translational motion in the imaging plane, speckle patterns will move in the imaging plane. In this case, spatial cross-correlation analysis, similar to that used in DPIV, can be applied to track speckle features and infer in-plane, translational motion. The application of feature tracking to an imaging system characterized by speckle is known as speckle tracking [42, 55, 56].

Like in DPIV, if the particles that generate the speckle pattern move orthogonal to the imaging plane, then the speckle patterns will change over time. As particles diffuse relative to one another, the speckle patterns will also change, making feature tracking more difficult. Thus imaging frame rates should be fast enough to track features before they change due to diffusion or out-of-plane motion.

Point-based (0D) approaches

While imaging-based approaches exploit spatial information to identify particles or features and track them, flow information can also be inferred by analyzing the time-varying signal at a single (0D) point.

Decorrelation-based approaches

Another method that exploits speckle for flow quantification is speckle decorrelation analysis. Diffusive and translational motion through an image pixel causes the signal from that (0D) point to decorrelate over time. The rate at which decorrelation occurs depends on how fast particles translate through the pixel, as well as how quickly particles diffuse. By fitting the rate of decorrelation to a mathematical model of decorrelation, the translational speed s and diffusivity D at the pixel location (x, y, z) can be estimated. If the signal originates from the backscattered light of particles in optical coherence tomography (OCT), then the analysis is known as dynamic light scattering (DLS)-OCT [57, 58]. Decorrelation-based OCT approaches have been applied toward imaging fluid speed and diffusion [59–61].

In contrast to speckle tracking, which uses spatial information for cross-correlation, 0D techniques rely on the temporal decorrelation of a signal at a single pixel. While only out-of-plane motion causes speckle patterns to change in speckle tracking, any type of translational motion will cause a signal at a single point to decorrelate. Diffusion causes the signal to decorrelate over time in both cases.

Fluorescence correlation spectroscopy and fluorescence recovery after photobleaching

In fluorescent imaging systems, a temporal analysis also can be applied to a 0D time signal. For example, if the

signal arises from a fluorescent molecule as imaged by a confocal microscope, then the technique is known as fluorescence correlation spectroscopy (FCS) [62]. In the case of FCS, decorrelation occurs due to translational or diffusive motion of dye molecules through a focus. The decorrelation of the signal can be fit to yield the translational speed s and diffusivity D [63]. In a related technique known as fluorescence recovery after photobleaching, the time-varying signal is fit to a model function predicted by the diffusion of fluorophores into a previously photobleached confocal volume, and diffusivity and flow speed can be recovered [64].

Doppler velocimetry

In Doppler velocimetry, the frequency shift of light due to the Doppler effect is measured to give an estimate of the axial component of flow (the component directed along the propagation path of light), denoted here as v_z , at some location (x, y, z) . As with the other OD approaches, the frequency shift is calculated from a time-varying signal at a single point. Doppler velocimetry is commonly used in ultrasound to measure blood flow and has also found use for blood flow imaging in OCT [65–67]. Because Doppler only captures a single velocity component v_z , however, and because cilia-driven fluid flow is typically parallel to the surface (that is containing primarily v_x and v_y components of flow), using Doppler alone has limitations for ciliary imaging. Recently, though, there has been work in developing more complex models of the OCT signal and incorporating Doppler into a framework that also includes methods for qualifying x - y (en face) flow [58, 68]. These methods hold promise for quantifying cilia-driven fluid flow.

Model systems of cilia-driven fluid flow

There are numerous model systems for studying ciliary flow ranging from human, to cell culture, to animal models, and each of these models has their own advantages and disadvantages [14, 23, 69–76]. Although a complete discussion of model systems of ciliary flow is outside the scope of this review, we would like to highlight two model systems we believe to have been important for imaging cilia-driven fluid flow.

The first model system is the frog embryo from the *Xenopus* genus (*Xenopus laevis* and *Xenopus tropicalis*). *Xenopus* species have traditionally been used to study embryonic development [77, 78]. They also, however, express cilia in multiple organ systems, and in particular a ciliated surface epithelium that is accessible with no dissection. Cilia-driven flow has been investigated in *Xenopus* epithelium, CSF

circulation [79], and embryonic nodal flow [80]. Simultaneously, many genetic manipulation techniques available for *Xenopus* are significantly faster to implement as compared to mammalian systems [81]. As such, *Xenopus* embryos are useful not only for readily imaging ciliary flow, but also for biologically manipulating ciliary flow in the context of respiratory disease, central nervous system disorders, and disorders of left–right patterning.

The second important model system is the air-liquid interface (ALI) in vitro model system [82, 83]. ALI cultures can be derived from vertebrate cells, including mouse and human, and extracted cells differentiate into both mucus-secreting goblet cells and ciliated epithelial cells. Because ALI cultures recapitulate both the mucus and ciliary component of respiratory flow and because cells can be cultured from patients with specific mutations, ALI cultures have proven to be very important in the study of ciliary disease [84].

Microscale imaging of cilia-driven fluid flow

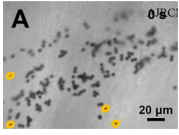
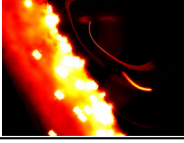
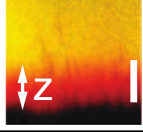
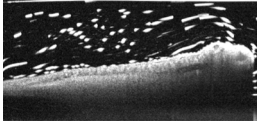
As shown in Fig. 3, there are many combinations of flow system, velocimetry technique, and imaging modality that have been used to image cilia-driven fluid flow. The choice of these categories, then, depends on several factors. One factor is the level of quantification required for the study. The various velocimetry techniques can achieve different degrees of measurement sophistication, ranging from differentiating flow versus no flow, to estimating linear flow speed, to fully quantifying the flow field. The level of quantification, in turn, depends on the physiological question to be investigated. Another consideration is that different optical imaging modalities have different advantages and disadvantages in terms of resolution, imaging speed, depth sectioning, and contrast.

As shown in Fig. 5, the bulk of microscopic ciliary flow imaging has been performed using four optical imaging techniques: traditional light microscopy, epifluorescence microscopy, confocal fluorescence microscopy, and optical coherence tomography (OCT). Historically, light microscopy was the most important. Since then, epifluorescence and confocal fluorescence have become the standard methods of measuring flow. More recently, however, OCT has shown great promise as a new method. In this section, we review applications of these various microscopic techniques toward ciliary flow imaging and discuss the advantages and disadvantages of each.

Light microscopy

Light microscopes were the first type of microscope to be invented, and they are still the most common microscope

Fig. 5 Commonly used optical techniques for investigating cilia-driven fluid flow, with advantages and disadvantages of each technique. *Top* Light microscopy has historically been used (image showing tracheal mucus velocity measurement, reproduced from [108]). *Middle* Epifluorescence (image showing epithelial ciliary flow, unpublished work from authors) and confocal fluorescence (image showing airway surface liquid, reproduced from [165]) are the current standard methods. *Bottom* Optical coherence tomography (image showing epithelial ciliary flow, unpublished work from authors) is an emerging method showing promise for flow quantification

Light Microscopy		Easy Implementation High Speed
		No Depth Sectioning No Molecular Specificity
Epifluorescence		Low Background High Speed
		No Depth Sectioning
Confocal Fluorescence		Low Background Depth Sectioning
		Slow Acquisition Speed Small Field of View
Optical Coherence Tomography		Depth Sectioning Parallelized Depth Acquisition
		Speckle Artifact No Molecular Specificity

Optical Techniques for Microscale Cilia-Driven Fluid Flow

available today. Here we denote any standard microscope that uses white light in either a transmissive or epi-illumination mode as light microscopy. Light microscopy uses intrinsic scattering and absorption of light by samples to provide contrast. Light microscopy is typically one of the simplest optical setups to implement, and, perhaps due to this simplicity, was historically an important modality for imaging cilia-driven fluid flow.

Epithelial imaging with light microscopy imaging

The first studies of cilia-driven fluid flow were performed using standard white light microscopes to visualize movement of a dye or track moving particles to estimate linear flow speed. As far back as the 1870s, in experiments involving amphibian epithelial models of ciliary flow, researchers visually tracked weights and timed movement with a stopwatch to determine linear flow speed [85, 86].

Even using this simple technique, early researchers made sophisticated measurements determining the amount of work that cilia could output as a function of ciliary load. It was shown, for example, that cilia increased work and oxygen consumption in response to increased loading, but only up to a certain threshold [87, 88]. Simple dyes such as carmine and India ink were used to qualitatively assess flow speed and path in amphibian models [89, 90] as well as in human (nasal cavity) and monkey, either in vivo or ex vivo [91, 92]. More standardization of protocol in particle tracking occurred in the 1930s, when carbon particles or sterilized spores were used as seed particles [93–95]. It was at this time that ciliary beat frequency was also studied

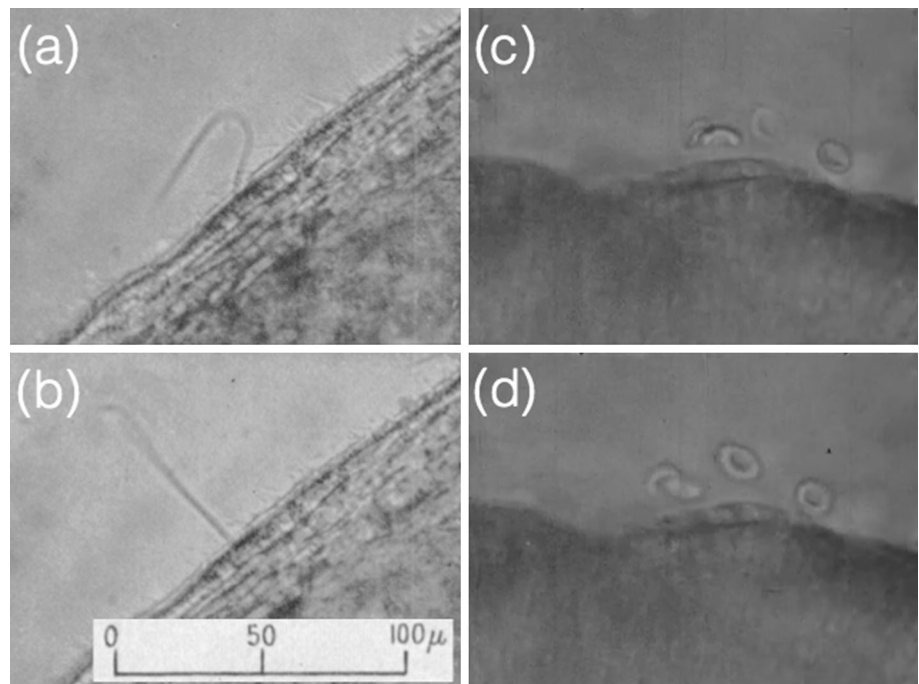
using light microscopy, including the use of 200 frames-per-second cinematography [90, 96, 97]. Figure 6 shows examples of such ciliary studies from the 1930s, demonstrating a high level of sophistication even 80 years ago.

Respiratory imaging with light microscopy

Since its initial implementation in the early 20th century, light microscopy has continued to be important for ciliary imaging in the respiratory tract. Light microscopy-based particle tracking and ciliary beat frequency measurements were refined in the 1950s and 60s [17, 98] and were later used to study the effects of pharmacological agents [99], air pollution [100], and smoking [101] on mucociliary flow. With the increasing use of bronchoscopy, other particles such as Teflon discs or charcoal could be seeded in the tracheas of large animal model and even humans to image in vivo mucociliary clearance [102] and CBF [103], allowing further study of the effects of drugs [104] and cigarette smoking [105, 106] on respiratory mucus clearance.

Even as more technically complex imaging modalities such as fluorescence microscopy and optical coherence tomography (discussed below) have come into more common use, light microscopy continues to play an important role in quantifying mucociliary flow speed. Researchers have used light microscopy to investigate physiological principles of flow and the role of mucus [74, 107–109], pharmacological and chemical signaling pathways [110–112], and the effects of infection on mucociliary clearance [113]. Moreover, there have been

Fig. 6 Early works in the videomicroscopic study of ciliary physiology. *Panels (a) and (b)* are two consecutive frames from a 200 frames-per-second movie of abfrontal cilia motion in *Mytilus edulis* (blue mussel). Images reproduced from [96], published in 1930. *Panels (c) and (d)* are closely spaced frames from a movie that captured cilia-driven fluid flow in a rabbit trachea. Red blood cells were used as flow tracers. Images are reproduced from [188], originally produced in 1934. The *scale bar in (b)* is for frames (a) and (b) only



continued technical developments to increase contrast in light microscope-type setups [114] to obtain higher quality images, as well as to use new types of metrics such as entropy to quantify mixing efficiency, as shown in Fig. 7 [115].

Oviduct imaging with light microscopy

Light microscopy has also played an important role in investigating other types of cilia-driven fluid flow. Beginning in the 1960s and 70s, light microscopy particle tracking approaches were initially implemented in imaging cilia-driven fluid flow in the oviduct [69, 116–119]. Oviduct flow results from the combination of ciliary motion, muscular contraction, and fluid production. Follow-up studies used light microscopy to elucidate the role of ciliary beating versus muscular contraction [120, 121], as well as the effects of sex hormones [122] and pharmacological agents [123] on flow. Notably, unlike the lungs and sinuses, the oviducts are not optically accessible without surgery, and thus studies were typically performed on ex vivo human or mammal tissue. Nonetheless, light microscopy continues to be important today for studying the role of cilia in the oviduct [4], including recent work on gamete transport [124–126].

Nodal imaging with light microscopy

The node is a transient structure that is present during a portion of embryonic life. Cilia in the node are thought to

rotate in a clockwise fashion to generate a leftward flow (Fig. 1 right), thereby creating asymmetric patterning signals [5]. Light microscopy has been used to study nodal flow [127], but it is used less commonly than epifluorescence, which will be discussed in the following section.

Limitations of light microscopy

Historically, the most common uses of light microscopy were to (1) qualitatively judge the presence or absence of flow or (2) manually track particles to estimate a linear flow speed, without directionality. For many experiments, this level of information sufficed to answer any relevant physiological questions. As researchers continue to investigate ciliary physiology in more detail, however, sometimes more complete descriptions of flow such as the vectorial flow field are required.

Although light microscopy can be used to measure a two-dimensional flow field, there are several limitations. First, even if two-component velocimetry can be implemented, it may not be sufficient to fully characterize flow. In applications such as the lung and the oviduct, flow is confined geometrically by the tube-like structures of the trachea or oviduct, and knowledge of two-component flow in combination with the orientation of the tube often allows full characterization of flow. In less constrained geometries such as the CSF, node, or epithelium of amphibian models, however, flow may not be directed exactly parallel to the ciliated surface. In these cases, full characterization of flow requires estimation of three-component flow fields.

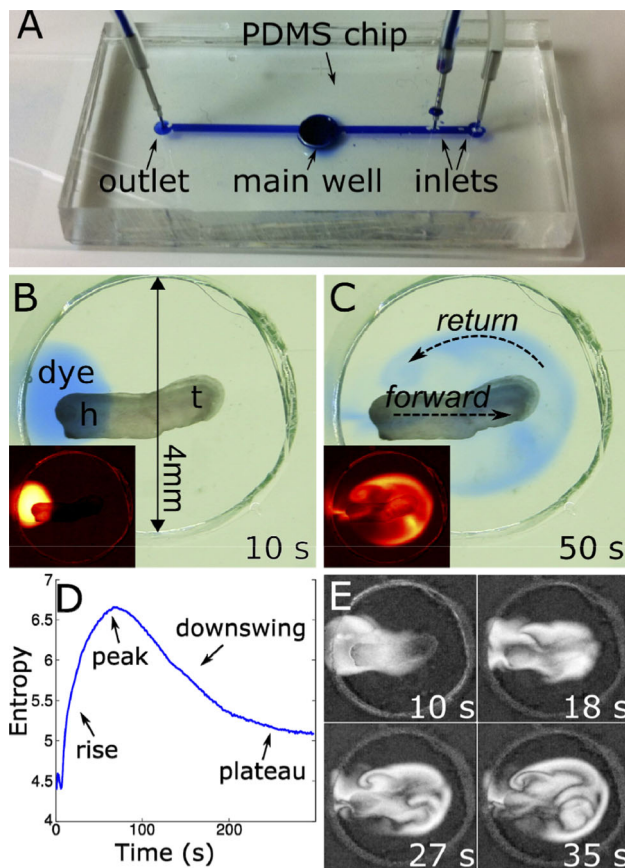


Fig. 7 Quantification of ciliary performance using light microscopy and entropy of dye mixing, reproduced from [115]. (a) Microfluidic chip layout; (b, c) time evolution of mixing process, false color insets show contrast-enhanced flow patterns; (d) time-varying image entropy, a measure of flow performance; (e) maps of local entropy, another measure of flow performance

More practically speaking, two-dimensional particle tracking velocimetry can be challenging to reliably implement with light microscopy. Because light microscopy does not have optical sectioning capabilities [128], tracked particles cannot always be localized to a specific depth. In addition, particle tracking velocimetry requires the ability to identify individual particles, which in turn requires imaging contrast between particles and the surrounding fluid. Although standard reflective light microscopy was sufficient for early experiments, it became apparent that the mucus in the lungs itself refracted and scattered light, making it difficult to resolve tracer particles from the surrounding environment [129]. Thus, in certain cases, light microscopy may not provide sufficient imaging contrast to reliably identify particles from background.

These limitations of light microscopy were addressed by subsequent developments in optical techniques. Fluorescent-based methods overcame the imaging contrast limitation by eliminating non-specific background.

Methods such as confocal microscopy and optical coherence tomography addressed the limitation in optical sectioning by (1) employing mechanisms for rejecting out-of-focus light and (2) quantitatively localizing every pixel in three-dimensional space.

Fluorescence microscopy

Fluorescence microscopy refers to any microscopic implementation that involves excitation of fluorophores with light and formation of an image by detection of the emitted light. In the context of ciliary flow imaging, fluorescence tends to take two forms: epifluorescence and confocal fluorescence. Epifluorescence refers to the fluorescent excitation of a large area of a sample and the imaging of the emitted fluorescence with a camera. Like standard light microscopy, epifluorescence does not offer any depth sectioning.

Confocal fluorescence, on the other hand, refers to microscope setups in which fluorescent light is only collected from a very small focal volume. Most confocal fluorescent setups scan a microscope focus over a sample and reconstruct an image in a point-wise fashion. Because fluorescent emission is localized to a specific location, determined by the pinhole of the microscope, confocal fluorescent images are by their nature cross-sectional and provide optical sectioning.

Epifluorescence microscopy

Epifluorescence offers extremely low background and thus high specificity imaging contrast [130]. Indeed, although mucus can be auto-fluorescent, the use of fluorescently labeled microspheres offers increased contrast between mucus and tracer when compared to standard light microscopy [20, 129], and is thus attractive for implementing particle tracking and related techniques. In addition, fluorescent techniques in general allow multiplexing of chemical labeling based on different fluorophores. Although epifluorescence does not offer depth sectioning, if particles are seeded sparsely, particle tracking velocimetry can be implemented successfully.

Epithelial imaging with epifluorescence

Epifluorescent particle tracking velocimetry was first implemented by Winet et al. [129] to study flow in the ciliated epithelium in frog. They were able to quantify vectorial flow in a mucus preparation seeded with fluorescent beads and later use depth-dependent changes in flow to calculate shear stress [131]. After the initial demonstrations, epifluorescent techniques continued to be important in studying the ciliated epithelium of amphibian

models [20]. For example, one important ongoing research question in ciliary physiology is how ciliated surfaces develop directional flow. Quantifying directional flow development by its very nature requires making directional, vectorial measurements of velocity. Epifluorescent imaging was used for a series of studies in *Xenopus laevis* that investigated the interplay between tissue patterning, already known to be important in embryonic life [132], and subsequent development of flow directionality [19, 21, 133].

Respiratory imaging with epifluorescence

Epifluorescent-based particle tracking has been very important in studying mucus flow in the respiratory tract [72]. It has been used to study the effects of mucus removal on flow [107, 108], the effects of physiological stressors [134], and development of directional flow in the trachea [135]. It also became the primary method of estimating mucus velocity in bronchoepithelial cell culture [22, 136–138]. Although the most common implementation of epifluorescence is particle tracking of beads, other methods such as tracing out streaks in time lapse [22] or digital particle image velocimetry in more densely seeded media [139] have also been implemented in respiratory imaging.

Nodal flow imaging with epifluorescence

Most studies of cilia-driven fluid flow in the node have used epifluorescence to quantify flow [140, 141]. Important studies have been performed to study the effects of knocking out specific genes such as *kif3a* [142], *kif3b* [143], and *dnah9* [144]. Epifluorescent imaging was also used to study the fluidic dynamics of the node in mammalian [40, 145], zebrafish [146, 147], amphibian [80], and artificial cilia systems [148].

Cerebrospinal fluid (CSF) imaging with epifluorescence

CSF flow is thought to be driven by three factors: the production and drainage of CSF, vascular pulsations, and ciliary action [149–151]. Although it is known that patients with ciliary defects developed hydrocephalus [7, 152, 153], the exact degree to which cilia contribute to CSF flow remains an open question. Imaging of CSF flow with fluorescence, either by injection of beads in vivo [79] or by dissection of the ventricles is helping to elucidate the role that cilia play in CSF flow. Epifluorescent particle and dye tracking have since been used to investigate defects in genes such as *mdnah5* [154] and *tg737* [155], to characterize normal development of CSF flow [146, 156], and to study the role of tissue patterning in the development of flow directionality [157].

Oviduct imaging with epifluorescence

Epifluorescence has also been used to image oviduct flow [124], but its use in the oviduct appears to be more limited than light microscopy. This may be due to the fact that ova themselves are often tracked in the oviduct, which minimizes the need for seeding fluorescent tracers.

Limitations of epifluorescence

In epifluorescence, as in light microscopy, light emanating from out-of-focus point objects is blurred but not rejected, and light from out-of-focus particles can enter the image. Careful experiments have been able to identify in-plane particles to reconstruct flow profiles [129, 131], but the techniques are limited by (1) the fact that there is no genuine localization and (2) there is potentially significant amounts of defocused, out-of-plane signal preventing particle identification unless particles are very sparse. For these reasons, if vectorial flow information is desired, then confocal and OCT imaging systems, which are cross-sectional in nature, may offer more robust depth localization for flow field estimation.

Confocal fluorescent microscopy

Confocal fluorescent microscopy uses a pinhole to reject out-of-plane light and offers true depth sectioning [158] with spatial resolution of less than 1 μm [128]. Because it combines the low background and molecular specificity of fluorescence with the cross-sectional nature of confocal microscopy, confocal fluorescence became a very attractive technique especially for imaging the layered airway surface liquid (ASL).

Respiratory imaging with confocal

The first use of confocal fluorescent microscopy in cilia-driven fluid flow that we could identify comes from Matsui et al. They labeled the airway surface liquid with fluorescently tagged dextrans and used confocal microscopy to image the clearance of dye from a small area where caged fluorophores had been released [22], a technique similar to molecular tagging velocimetry. In this study, the high resolution of confocal microscopy was leveraged to demonstrate a novel physiological finding with regard to the airway surface liquid. While the periciliary layer was previously thought to be non-flowing, the authors found that indeed both the mucus layer and the periciliary layer underwent the same rate of fluid transport.

Building on this work, researchers continued to use confocal fluorescence to image the airway surface liquid and showed, for example, the importance of defects in regulating

airway surface liquid depth in cystic fibrosis [159–163]. Fluorescence microscopy also offers the major advantage that the layers of the airway surface liquid can be labeled with either antibody [84, 164, 165] or chemical probes [138], thus allowing differentiation of mucus layer from periciliary layer. Because of the ability to differentiate the layers, confocal microscopy was also used to study compartmental transport between the mucus and periciliary layer [137, 165].

Because confocal microscopy requires point scanning, imaging frame rates are generally slower than epifluorescence. PTV requires sufficiently high frame rates needed to accurately track particles. This speed limitation of scanning confocal may explain why although particle tracking velocimetry has been implemented in mucociliary flow imaging [166], the more common implementation of confocal fluorescence appears to be in static imaging of airway surface liquid structure [136].

Oviduct and nodal imaging with confocal

Confocal fluorescence-based particle tracking has been applied toward imaging flow in the oviduct [167, 168]. With regard to nodal imaging, Supatto et al. [169] used femtosecond laser ablation to generate fluorescent debris within Kupffer's vesicle, the analogous structure of the node in zebrafish embryo. They used three-dimensional confocal imaging to generate three-dimensional, three-component velocity vector fields (Fig. 4) and showed that flow can be either directional or vortical, depending on depth. Because vorticity cannot be calculated without directional velocity components, their work underscores the importance of three-component velocity imaging.

Other confocal-based measurements: ciliary beat frequency, fluorescence recovery after photobleaching, and fluorescence correlation spectroscopy

Due to its high resolution and well defined focal volume, confocal fluorescent microscopy offers the ability to measure additional quantities related to ciliary beat frequency and diffusivity. Because cilia themselves can be fluorescently labeled, using a rapid enough confocal microscope allows quantification of ciliary beat frequency by direct visualization of the cilia themselves [20, 166, 170]. Moreover, methods of measuring diffusivity such as fluorescent recovery after photobleaching (FRAP) and fluorescence correlation spectroscopy (FCS) require well-defined, reasonably Gaussian focal volumes to properly extract diffusion [64, 171]. Indeed, FRAP has been used to interrogate the diffusivity of mucus layer versus periciliary layer in cystic fibrosis versus non-cystic fibrosis patients [172], and FCS has been used to quantify diffusivity of viruses in cervical mucus [173].

Limitations of confocal

Confocal fluorescence has allowed for the elucidation of important mucociliary physiology and will likely continue to be essential to microfluidic ciliary flow imaging. Nonetheless, it suffers from a limitation arising from scanning. In most confocal setups, the signal from just a single focus is recorded at any given time. That focus is then scanned in the xy -plane (the en face plane), and the process is repeated in the axial direction (the z -axis, along which light propagates) to acquire an entire volume [174].

Scanning can be performed in the xy -plane through the use of galvanometric mirrors with no physical attachment to the sample or objective. For scanning in the z -dimension, however, most setups require physical scanning of either the objective or the sample, usually with a piezoelectric element. That mechanical scanning can itself perturb the sample [175]. Due to experimental considerations, the airway surface liquid must be imaged from above [129], meaning that to resolve the layered structure, scanning must occur in the z -dimension. In addition, for volumetric particle tracking, scanning must necessarily occur in the z -dimension. Overall, then, axial scanning is important for ciliary flow imaging but is currently a limitation of confocal microscopy. The ability to image axially without mechanically scanning is one important advantage of optical coherence tomography.

Optical coherence tomography

Optical coherence tomography (OCT) [176–178] is a microscopic imaging technique that uses the low temporal coherence light to perform depth ranging. It is often considered the light-based analog of ultrasound. Axial resolution in OCT is typically in the ~ 3 – 10 μm regime. The axial resolution is determined by the center wavelength and bandwidth of the light source, two parameters that determine the temporal coherence length of the light source. Lateral resolution in OCT is typically in ~ 5 – 20 μm regime. In comparison, conventional confocal microscopy typically has spatial resolution in the micron to sub-micron regime. The major advantage of OCT over confocal, however, is that OCT inherently parallelizes acquisition in the z -dimension, thus eliminating the need for mechanical z -scanning.

OCT has additional advantages over confocal microscopy, as well. Because objective lenses with longer focal lengths are used, typical OCT setups have a long working distance objective of ~ 2 – 3 cm, eliminating any possibility that the ciliary flow system is affected by the physical presence of the microscope objective. OCT also has the ability to interferometrically reject multiply scattered

photons, allowing for relatively deep tissue imaging ($\sim 1\text{--}2$ mm). Similar to non-fluorescence, reflectance confocal microscopy, OCT uses differences in backscattered light as contrast, thus allowing for the possibility of label-free mucus imaging. Finally, OCT is a coherent detection method, allowing implementation of Doppler flow imaging. Because of these advantages of OCT over confocal fluorescent microscopy, there has been a great deal of recent interest in applying OCT toward imaging cilia-driven fluid flow.

Optical coherence tomography-based feature tracking

In 2011, Jonas et al. showed the first implementation of OCT in cilia-driven fluid flow. In this work, they implemented particle tracking velocimetry on polystyrene microspheres driven by the ciliated skin of *Xenopus* embryos [179]. Because acquisition was inherently depth resolved, they were able to quantify the flow vector field in two dimensions (xz -plane) and show that the flow speed and directionality varied significantly as a function of the distance from the ciliated surface. These findings again reinforced the importance of both directional and depth-resolved velocity measurements.

Mucus inherently backscatters light and is composed of many particles that generate a speckle pattern. A second application of OCT toward mucociliary flow imaging involved the use of speckle tracking to calculate the two-dimensional flow field of mucus in air-liquid interface cultures [180]. Oldenburg et al. were able to show label-free, directional measurement of mucociliary flow in a depth-resolved manner. In addition, they were able to use time-dependent signals, similar to analysis in light scattering-based approaches, to quantify relative changes in ciliary beat frequency (CBF) due to gaseous anesthetic. Notably, however, they were unable to measure absolute CBF, likely because spatial resolution was not sufficiently high.

μ OCT for mucociliary imaging

Most OCT systems have tradeoff between lateral resolution and axial field of view. That is, one can increase lateral resolution by increasing the numerical aperture of the objective lens to increase light focusing, but the axial field of view (FOV) decreases simultaneously. For a typical OCT system, lateral resolution may be ~ 10 μm , while axial FOV is ~ 2 mm. Liu et al. were able to circumvent this tradeoff using extended depth of focus imaging sources [181] to extend high lateral resolution (~ 1 μm) imaging over a ~ 1 mm FOV [182]. Consequently, they were able to use their μ OCT system to image the layered airway surface liquid structure with

confocal-level resolution, as shown in Fig. 8 [183]. They were able to achieve high enough resolution to image individual cilia to make absolute CBF measurements, while simultaneously using manual feature tracking on the mucus layer to estimate mucociliary flow. In a follow-up study, they used μ OCT methods to investigate the effects of mucus loading on CBF and periciliary layer height [184]. Overall, their methods demonstrated that OCT is capable of simultaneously imaging the layered structure of the airway surface liquid and cilia themselves simultaneously.

Dynamic light scattering OCT

As described in “[Point-based \(0D\) approaches](#)”, point-based methods such as dynamic light scattering can be used to quantify the rate of decorrelation at a given location and estimate fluid flow speed [58]. Such approaches, in combination with Doppler velocimetry, have been proposed as an alternative technique for quantifying directional cilia-driven flow velocity with OCT [68]. Moreover, DLS–OCT has been used to quantify localized diffusion in the mucus of air-liquid interface culture [49, 185]. Thus, we believe that OCT holds promise in quantifying both flow and diffusion in ciliary systems.

Limitations of OCT

OCT has already shown excellent results in imaging cilia-driven fluid flow, but it does suffer from limitations. As previously mentioned, OCT has lower resolution than confocal microscopy. In addition, much like light microscopy, image contrast in OCT arises from differences in light scattering, and thus it lacks the chemical specificity of fluorescence microscopy. Currently, however, there is development underway to combine OCT with more molecular specific imaging modalities such as Raman spectroscopy to achieve molecular specific signals [186]. As these dual modality techniques mature, they may also find a place in cilia-driven flow imaging.

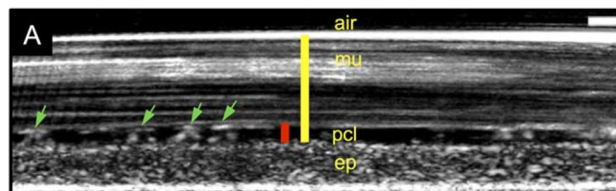


Fig. 8 Micro-optical coherence tomography (μ OCT) image showing airway surface liquid, reproduced from [183]. OCT can be used to differentiate the mucus layer (mu), periciliary layer (pcl), and individual cilia (green arrows) in relation to epithelial cell layer (ep)

Conclusions

Cilia-driven fluid flow is an important physiological process in multiple organ systems, including the respiratory tract, the oviduct, the ventricles of the brain, and the embryonic node. Defects in cilia-driven fluid flow have significant health ramifications, and thus quantifying fluid flow in these systems is of great importance. General methods of velocimetry can be divided into particle versus dye-based techniques, as well as techniques which rely on 2D or 3D imaging versus those which can be performed using the signal from a single point (0D).

These velocimetry techniques have been combined primarily with four optical modalities to study microfluidic flow: light microscopy, epifluorescence, confocal fluorescence, and optical coherence tomography. Light microscopy has historically been the most important modality for quantifying ciliary flow but has been partially replaced by epifluorescence and confocal fluorescence microscopy, which are the current standards. Optical coherence tomography, a high-speed, cross-sectional microscopic imaging modality, has recently shown great promise as an emerging method for microscale imaging of cilia-driven fluid flow. Advances in imaging speed and resolution will continue to drive advances in cilia flow physiology.

Acknowledgments We thank Ute Gamm for her useful feedback. This work was supported by a March of Dimes Basil O'Connor Starter Scholar Research Award and NIH 1R01HL118419-01. BKH also was supported by NIH MSTP TG T32GM07205.

References

- Meyer K (2002) Lung immunology and host defense. In: Bittar EE (ed) Pulmonary biology in health and disease. Springer, New York, pp 332–345. doi:[10.1007/978-0-387-22435-0_18](https://doi.org/10.1007/978-0-387-22435-0_18)
- Rowe SM, Miller S, Sorscher EJ (2005) Cystic fibrosis. *N Engl J Med* 352(19):1992–2001. doi:[10.1056/NEJMra043184](https://doi.org/10.1056/NEJMra043184)
- Stillwell PC, Wartchow EP, Sagel SD (2011) Primary ciliary dyskinesia in children: a review for pediatricians, allergists, and pediatric pulmonologists. *Pediatric allergy, immunology, and pulmonology* 24(4):191–196. doi:[10.1089/ped.2011.0099](https://doi.org/10.1089/ped.2011.0099)
- Lyons RA, Saridogan E, Djahanbakhch O (2006) The reproductive significance of human Fallopian tube cilia. *Human reproduction update* 12(4):363–372. doi:[10.1093/humupd/dml012](https://doi.org/10.1093/humupd/dml012)
- Brueckner M (2007) Heterotaxia, congenital heart disease, and primary ciliary dyskinesia. *Circulation* 115(22):2793–2795. doi:[10.1161/CIRCULATIONAHA.107.699256](https://doi.org/10.1161/CIRCULATIONAHA.107.699256)
- Spassky N (2013) Motile cilia and brain function: ependymal motile cilia development, organization, function and their associated pathologies. In: Tucker KL, Caspary T (eds) Cilia and nervous system development and function. Springer, Netherlands, pp 193–207. doi:[10.1007/978-94-007-5808-7_7](https://doi.org/10.1007/978-94-007-5808-7_7)
- Ibanez-Tallon I, Heintz N, Omran H (2003) To beat or not to beat: roles of cilia in development and disease. *Human Mol Genet* 12(Spec No 1):R27–R35
- Haimo LT, Rosenbaum JL (1981) Cilia, flagella, and microtubules. *The Journal of cell biology* 91(3 Pt 2):125s–130s
- Cooper GM (2000) The cytoskeleton and cell movement. In: The cell: a molecular approach, 2nd edn. ASM Press; Sinauer Associates, Washington, DC Sunderland, Mass., pp xxiv, p 689
- Fawcett DW, Porter KR (1954) A study of the fine structure of ciliated epithelia. *J Morphol* 94(2):221–282. doi:[10.1002/jmor.1050940202](https://doi.org/10.1002/jmor.1050940202)
- Bellomo D, Lander A, Harragan I, Brown NA (1996) Cell proliferation in mammalian gastrulation: the ventral node and notochord are relatively quiescent. *Dev Dynam* 205(4):471–485. doi:[10.1002/\(Sici\)1097-0177\(199604\)205:4<471::Aid-Aja10>3.0.Co;2-4](https://doi.org/10.1002/(Sici)1097-0177(199604)205:4<471::Aid-Aja10>3.0.Co;2-4)
- Gibbons IR, Rowe AJ (1965) Dynein—a protein with adenosine triphosphatase activity from cilia. *Science* 149(3682):424–426. doi:[10.1126/Science.149.3682.424](https://doi.org/10.1126/Science.149.3682.424)
- Satir P, Sleight MA (1990) The physiology of cilia and mucociliary interactions. *Annu Rev Physiol* 52:137–155. doi:[10.1146/annurev.ph.52.030190.001033](https://doi.org/10.1146/annurev.ph.52.030190.001033)
- Antunes MB, Cohen NA (2007) Mucociliary clearance—a critical upper airway host defense mechanism and methods of assessment. *Curr Opin Allergy Clin Immunol* 7(1):5–10. doi:[10.1097/ACI.0b013e32801144ef](https://doi.org/10.1097/ACI.0b013e32801144ef)
- Sleight MA, Blake JR, Liron N (1988) The propulsion of mucus by cilia. *Am Rev Respir Dis* 137(3):726–741. doi:[10.1164/ajrccm/137.3.726](https://doi.org/10.1164/ajrccm/137.3.726)
- Dalhamn T, Rylander R (1962) Frequency of ciliary beat measured with a photo-sensitive cell. *Nature* 196:592–593
- Dalhamn T (1960) The determination in vivo of the rate of ciliary beat in the trachea. *Acta Physiol Scand* 49:242–250. doi:[10.1111/j.1748-1716.1960.tb01949.x](https://doi.org/10.1111/j.1748-1716.1960.tb01949.x)
- Marino MR, Aiello E (1982) Cinemicrographic analysis of beat dynamics of human respiratory cilia. *Prog Clin Biol Res* 80:35–39
- Werner ME, Hwang P, Huisman F, Taborek P, Yu CC, Mitchell BJ (2011) Actin and microtubules drive differential aspects of planar cell polarity in multiciliated cells. *J Cell Biol* 195(1):19–26. doi:[10.1083/Jcb.201106110](https://doi.org/10.1083/Jcb.201106110)
- Werner ME, Mitchell BJ (2013) Using *Xenopus* skin to study cilia development and function. *Method Enzymol* 525:191–217. doi:[10.1016/B978-0-12-397944-5.00010-9](https://doi.org/10.1016/B978-0-12-397944-5.00010-9)
- Mitchell B, Jacobs R, Li J, Chien S, Kintner C (2007) A positive feedback mechanism governs the polarity and motion of motile cilia. *Nature* 447(7140):97–101. doi:[10.1038/nature05771](https://doi.org/10.1038/nature05771)
- Matsui H, Randell SH, Peretti SW, Davis CW, Boucher RC (1998) Coordinated clearance of periciliary liquid and mucus from airway surfaces. *J Clin Invest* 102(6):1125–1131. doi:[10.1172/JCI2687](https://doi.org/10.1172/JCI2687)
- King M (1998) Experimental models for studying mucociliary clearance. *Eur Respir J* 11(1):222–228
- Wu DX, Lee CY, Uyekubo SN, Choi HK, Bastacky SJ, Widdicombe JH (1998) Regulation of the depth of surface liquid in bovine trachea. *Am J Physiol* 274(3 Pt 1):L388–L395
- Berg HC (1993) Movement of self-propelled objects. In: Random walks in biology. Expanded edn. Princeton University Press, Princeton, p 152
- Squires TM, Quake SR (2005) Microfluidics: fluid physics at the nanoliter scale. *Rev Mod Phys* 77(3):977–1026. doi:[10.1103/Revmodphys.77.977](https://doi.org/10.1103/Revmodphys.77.977)
- Ovalle WK, Nahirney PC, Netter FH (2013) Netter's essential histology, 2nd edn. Elsevier/Saunders, Philadelphia
- Hunter RF (1988) Development of the fallopian tubes and their functional anatomy. The fallopian tubes. Springer, Berlin, pp 12–29. doi:[10.1007/978-3-642-73045-0_2](https://doi.org/10.1007/978-3-642-73045-0_2)
- Rutland J, Cole PJ (1981) Nasal mucociliary clearance and ciliary beat frequency in cystic fibrosis compared with sinusitis and bronchiectasis. *Thorax* 36(9):654–658
- Fernstrom I (1971) A new method for studying the motility of the Fallopian tubes. *Acta Obstet Gynecol Scand* 50(2):129–133

31. Hoegger MJ, Awadalla M, Namati E, Itani OA, Fischer AJ, Tucker AJ, Adam RJ, McLennan G, Hoffman EA, Stoltz DA, Welsh MJ (2014) Assessing mucociliary transport of single particles in vivo shows variable speed and preference for the ventral trachea in newborn pigs. *Proc Natl Acad Sci USA* 111(6):2355–2360. doi:[10.1073/pnas.1323633111](https://doi.org/10.1073/pnas.1323633111)
32. Hoegger MJ, Fischer AJ, McMenimen JD, Ostedgaard LS, Tucker AJ, Awadalla MA, Moninger TO, Michalski AS, Hoffman EA, Zabner J, Stoltz DA, Welsh MJ (2014) Cystic fibrosis. Impaired mucus detachment disrupts mucociliary transport in a piglet model of cystic fibrosis. *Science* 345(6198):818–822. doi:[10.1126/science.1255825](https://doi.org/10.1126/science.1255825)
33. Kambe T (2007) Flows. In: *Elementary fluid mechanics*. World Scientific, Hackensack, pp xv, p 386
34. Grant I (1997) Particle image velocimetry: a review. *P I Mech Eng C-J Mec* 211(1):55–76. doi:[10.1243/0954406971521665](https://doi.org/10.1243/0954406971521665)
35. Merzkirch W (2007) Flow visualization. In: Tropea C, Yarin A, Foss J (eds) *Springer handbook of experimental fluid mechanics*. Springer, Berlin, pp 857–870. doi:[10.1007/978-3-540-30299-5_11](https://doi.org/10.1007/978-3-540-30299-5_11)
36. Grubb BR, Jones JH, Boucher RC (2004) Mucociliary transport determined by in vivo microdialysis in the airways of normal and CF mice. *Am J Physiol Lung Cell Mol Physiol* 286(3):L588–L595. doi:[10.1152/ajplung.00302.2003](https://doi.org/10.1152/ajplung.00302.2003)
37. McKeon B, Comte-Bellot G, Foss J, Westerweel J, Scarano F, Tropea C, Meyers J, Lee J, Cavone A, Schodl R, Koochesfahani M, Andreopoulos Y, Dahm W, Mullin J, Wallace J, Vukoslavčević P, Morris S, Pardyjak E, Cuerva A (2007) Velocity, vorticity, and mach number. In: Tropea C, Yarin A, Foss J (eds) *Springer handbook of experimental fluid mechanics*. Springer, Berlin Heidelberg, pp 215–471. doi:[10.1007/978-3-540-30299-5_5](https://doi.org/10.1007/978-3-540-30299-5_5)
38. Sinton D (2004) Microscale flow visualization. *Microfluid Nanofluid* 1(1):2–21. doi:[10.1007/S10404-004-0009-4](https://doi.org/10.1007/S10404-004-0009-4)
39. Berg HC (1993) Diffusion: microscopic theory. In: *Random walks in biology*. Expanded edn. Princeton University Press, Princeton, p 152
40. Okada Y, Takeda S, Tanaka Y, Izpisua Belmonte JC, Hirokawa N (2005) Mechanism of nodal flow: a conserved symmetry breaking event in left-right axis determination. *Cell* 121(4):633–644. doi:[10.1016/j.cell.2005.04.008](https://doi.org/10.1016/j.cell.2005.04.008)
41. Schneider CA, Rasband WS, Eliceiri KW (2012) NIH Image to ImageJ: 25 years of image analysis. *Nat Methods* 9(7):671–675
42. Adrian RJ (1991) Particle-imaging techniques for experimental fluid-mechanics. *Annu Rev Fluid Mech* 23:261–304. doi:[10.1146/Annurev.Fluid.23.1.261](https://doi.org/10.1146/Annurev.Fluid.23.1.261)
43. M Raffel CW, Kompenhans J (1998) Three-component PIV measurements on planar domains In: *Particle image velocimetry: a practical guide*. Springer, New York
44. Prasad AK, Adrian RJ (1993) Stereoscopic particle image velocimetry applied to liquid flows. *Exp Fluids* 15(1):49–60
45. Raffel M, Westerweel J, Willert C, Gharib M, Kompenhans J (1996) Analytical and experimental investigations of dual-plane particle image velocimetry. *Opt Eng* 35(7):2067–2074. doi:[10.1117/1.600695](https://doi.org/10.1117/1.600695)
46. Dadi M, Stanislas M, Rodriguez O, Dymnt A (1991) A study by holographic velocimetry of the behavior of free small particles in a flow. *Exp Fluids* 10(5):285–294
47. Cierpka C, Kahler CJ (2012) Particle imaging techniques for volumetric three-component (3D3C) velocity measurements in microfluidics. *J Visual-Japan* 15(1):1–31. doi:[10.1007/S12650-011-0107-9](https://doi.org/10.1007/S12650-011-0107-9)
48. M Raffel CW, Kompenhans J (1998) Physical and technical background. In: *Particle image velocimetry: a practical guide*. Springer, New York
49. Chhetri RK, Blackmon RL, Wu WC, Hill DB, Button B, Casbas-Hernandez P, Troester MA, Tracy JB, Oldenburg AL (2014) Probing biological nanotopology via diffusion of weakly constrained plasmonic nanorods with optical coherence tomography. *Proc Natl Acad Sci USA* 111(41):E4289–E4297. doi:[10.1073/pnas.1409321111](https://doi.org/10.1073/pnas.1409321111)
50. Qian H, Sheetz MP, Elson EL (1991) Single-particle tracking—analysis of diffusion and flow in 2-dimensional systems. *Biophys J* 60(4):910–921
51. Berg HC (1993) Diffusion with drift. In: *Random walks in biology*. Expanded edn. Princeton University Press, Princeton, p 152
52. Willert CE, Gharib M (1991) Digital particle image velocimetry. *Exp Fluids* 10(4):181–193
53. Olsen MG, Adrian RJ (2000) Brownian motion and correlation in particle image velocimetry. *Opt Laser Technol* 32(7–8):621–627. doi:[10.1016/S0030-3992\(00\)00119-5](https://doi.org/10.1016/S0030-3992(00)00119-5)
54. Goodman JW (1985) Effects of partial coherence on imaging systems. In: *Statistical optics*. Wiley series in pure and applied optics. Wiley, New York, pp xvii, 550 p
55. Robinson DE, Chen F, Wilson LS (1982) Measurement of velocity of propagation from ultrasonic pulse-echo data. *Ultrasound Med Biol* 8(4):413–420. doi:[10.1016/S0301-5629\(82\)80009-4](https://doi.org/10.1016/S0301-5629(82)80009-4)
56. Trahey GE, Allison JW, Vonramm OT (1987) Angle independent ultrasonic-detection of blood-flow. *IEEE T Bio-Med Eng* 34(12):965–967. doi:[10.1109/Tbme.1987.325938](https://doi.org/10.1109/Tbme.1987.325938)
57. Berne BJ, Pecora R (2000) *Dynamic light scattering: with applications to chemistry, biology, and physics*. Dover edn. Dover Publications, Mineola
58. Lee J, Wu W, Jiang JY, Zhu B, Boas DA (2012) Dynamic light scattering optical coherence tomography. *Opt Express* 20(20):22262–22277. doi:[10.1364/OE.20.022262](https://doi.org/10.1364/OE.20.022262)
59. Boas DA, Bizheva KK, Siegel AM (1998) Using dynamic low-coherence interferometry to image Brownian motion within highly scattering media. *Opt Lett* 23(5):319–321. doi:[10.1364/Ol.23.000319](https://doi.org/10.1364/Ol.23.000319)
60. Kalkman J, Sprik R, van Leeuwen TG (2010) Path-length-resolved diffusive particle dynamics in spectral-domain optical coherence tomography. *Phys Rev Lett* 105(19):1983. doi:[10.1103/Physrevlett.105.198302](https://doi.org/10.1103/Physrevlett.105.198302)
61. Broillet S, Sato A, Geissbuehler S, Pache C, Bouwens A, Lasser T, Leutenegger M (2014) Optical coherence correlation spectroscopy (OCCS). *Opt Express* 22(1):782–802. doi:[10.1364/Oe.22.000782](https://doi.org/10.1364/Oe.22.000782)
62. Magde D, Webb WW, Elson E (1972) Thermodynamic fluctuations in a reacting system—measurement by fluorescence correlation spectroscopy. *Phys Rev Lett* 29(11):705. doi:[10.1103/Physrevlett.29.705](https://doi.org/10.1103/Physrevlett.29.705)
63. Kohler RH, Schwille P, Webb WW, Hanson MR (2000) Active protein transport through plastid tubules: velocity quantified by fluorescence correlation spectroscopy. *J Cell Sci* 113(22):3921–3930
64. Yguerabide J, Schmidt JA, Yguerabide EE (1982) Lateral mobility in membranes as detected by fluorescence recovery after photobleaching. *Biophys J* 40(1):69–75. doi:[10.1016/S0006-3495\(82\)84459-7](https://doi.org/10.1016/S0006-3495(82)84459-7)
65. Chen Z, Milner TE, Dave D, Nelson JS (1997) Optical Doppler tomographic imaging of fluid flow velocity in highly scattering media. *Opt Lett* 22(1):64–66
66. Izatt JA, Kulkarni MD, Yazdanfar S, Barton JK, Welch AJ (1997) In vivo bidirectional color Doppler flow imaging of picoliter blood volumes using optical coherence tomography. *Opt Lett* 22(18):1439–1441. doi:[10.1364/Ol.22.001439](https://doi.org/10.1364/Ol.22.001439)
67. Drexler W, Liu M, Kumar A, Kamali T, Unterhuber A, Leitgeb RA (2014) Optical coherence tomography today: speed, contrast, and multimodality. *J Biomed Opt* 19(7):071412. doi:[10.1117/1.JBO.19.7.071412](https://doi.org/10.1117/1.JBO.19.7.071412)
68. Huang BK, Choma MA (2014) Resolving directional ambiguity in dynamic light scattering-based transverse motion velocimetry

- in optical coherence tomography. *Opt Lett* 39(3):521–524. doi:[10.1364/Ol.39.000521](https://doi.org/10.1364/Ol.39.000521)
69. Blandau RJ, Boling JL, Halbert S, Verdugo P (1975) Methods for studying oviductal physiology. *Gynecol Obstet Inves* 6(3–4):123–145
 70. Felicetti SA, Wolff RK, Muggenburg BA (1981) Comparison of tracheal mucous transport in rats, guinea pigs, rabbits, and dogs. *J Appl Physiol Respir Environ Exerc Physiol* 51(6):1612–1617
 71. Tomkiewicz RP, Albers GM, De Sanctis GT, Ramirez OE, King M, Rubin BK (1995) Species differences in the physical and transport properties of airway secretions. *Can J Physiol Pharmacol* 73(2):165–171
 72. Robinson M, Bye PT (2002) Mucociliary clearance in cystic fibrosis. *Pediatr Pulmonol* 33(4):293–306
 73. Guilbault C, Saeed Z, Downey GP, Radzioch D (2007) Cystic fibrosis mouse models. *Am J Respir Cell Mol Biol* 36(1):1–7. doi:[10.1165/rcmb.2006-0184TR](https://doi.org/10.1165/rcmb.2006-0184TR)
 74. Rogers CS, Abraham WM, Brogden KA, Engelhardt JF, Fisher JT, McCray PB Jr, McLennan G, Meyerholz DK, Namati E, Ostedgaard LS, Prather RS, Sabater JR, Stoltz DA, Zabner J, Welsh MJ (2008) The porcine lung as a potential model for cystic fibrosis. *Am J Physiol Lung Cell Mol Physiol* 295(2):L240–L263. doi:[10.1152/ajplung.90203.2008](https://doi.org/10.1152/ajplung.90203.2008)
 75. Mall MA (2008) Role of cilia, mucus, and airway surface liquid in mucociliary dysfunction: lessons from mouse models. *J Aerosol Med Pulm Drug Deliv* 21(1):13–24. doi:[10.1089/jamp.2007.0659](https://doi.org/10.1089/jamp.2007.0659)
 76. Welsh MJ, Rogers CS, Stoltz DA, Meyerholz DK, Prather RS (2009) Development of a porcine model of cystic fibrosis. *Trans Am Clin Climatol Assoc* 120:149–162
 77. Werner ME, Mitchell BJ (2012) Understanding ciliated epithelia: the power of *Xenopus*. *Genesis* 50(3):176–185. doi:[10.1002/dvg.20824](https://doi.org/10.1002/dvg.20824)
 78. Assheton R (1896) Memoirs: notes on the ciliation of the ectoderm of the amphibian embryo. *Q J Microsc Sci* 2(152):465–484
 79. Miskevich F (2010) Imaging fluid flow and cilia beating pattern in *Xenopus* brain ventricles. *J Neurosci Meth* 189(1):1–4. doi:[10.1016/J.jneumeth.2010.02.015](https://doi.org/10.1016/J.jneumeth.2010.02.015)
 80. Schweickert A, Weber T, Beyer T, Vick P, Bogusch S, Feistel K (2006) Blum M (2007) Cilia-driven leftward flow determines laterality in *Xenopus*. *Curr Biol* 17(1):60–66. doi:[10.1016/J.Cub.10.067](https://doi.org/10.1016/J.Cub.10.067)
 81. Gilchrist MJ (2012) From expression cloning to gene modeling: the development of *Xenopus* gene sequence resources. *Genesis* 50(3):143–154. doi:[10.1002/dvg.22008](https://doi.org/10.1002/dvg.22008)
 82. Whitcutt MJ, Adler KB, Wu R (1988) A biphasic chamber system for maintaining polarity of differentiation of cultured respiratory tract epithelial cells. *In Vitro Cell Dev Biol* 24(5):420–428
 83. Gray TE, Guzman K, Davis CW, Abdullah LH, Nettesheim P (1996) Mucociliary differentiation of serially passaged normal human tracheobronchial epithelial cells. *Am J Respir Cell Mol Biol* 14(1):104–112. doi:[10.1165/ajrcmb.14.1.8534481](https://doi.org/10.1165/ajrcmb.14.1.8534481)
 84. Thornton DJ, Sheehan JK (2004) From mucins to mucus: toward a more coherent understanding of this essential barrier. *Proc Am Thorac Soc* 1(1):54–61. doi:[10.1513/pats.2306016](https://doi.org/10.1513/pats.2306016)
 85. Wyman J (1871) Experiments with Vibrating Cilia. In: Packard AS, Putnam FW (eds) *The American Naturalist*, vol V. Peabody Academy of Science, Salem, Mass, pp 611–616
 86. Bowditch HP (1876) Force of ciliary motion. *Boston Med Surg J* 95(6):159–164. doi:[10.1056/NEJM187608100950602](https://doi.org/10.1056/NEJM187608100950602)
 87. Maxwell SS (1905) The effect of salt-solutions on ciliary activity. *Am J Physiol* 13(2):154–170
 88. Gray J (1928) The Force exerted and the Work done by Cilia. In: *Ciliary movement*. Cambridge comparative physiology. Macmillan Co.; University Press, New York, p viii, p 162
 89. Gray J (1922) The mechanism of ciliary movement. *P R Soc Lond B-Conta* 93(650):104–121. doi:[10.1098/Rspb.1922.0007](https://doi.org/10.1098/Rspb.1922.0007)
 90. Lucas AM (1933) Principles underlying ciliary activity in the respiratory tract I. A method for direct observation of cilia in situ and its application. *Archiv Otolaryngol* 18(4):516–524
 91. Yates AL (1924) Methods of estimating the activity of the ciliary epithelium within the sinuses. *J Laryngol Otol* 39(10):554. doi:[10.1017/S0022215100026608](https://doi.org/10.1017/S0022215100026608)
 92. Lucas AM (1932) The nasal cavity and direction of fluid by ciliary movement in *Macacus rhesus* (Desm). *Am J Anat* 50(1):141–177. doi:[10.1002/Aja.1000500107](https://doi.org/10.1002/Aja.1000500107)
 93. Gray J (1923) The mechanism of ciliary movement III The effect of temperature. *P R Soc Lond B-Conta* 95(664):6–15. doi:[10.1098/Rspb.1923.0019](https://doi.org/10.1098/Rspb.1923.0019)
 94. Twitty VC (1928) Experimental studies on the ciliary action of amphibian embryos. *J Exp Zool* 50(3):319–344. doi:[10.1002/Jez.1400500302](https://doi.org/10.1002/Jez.1400500302)
 95. Lucas AM, Douglas LC (1934) Principles underlying ciliary activity in the respiratory tract II. A comparison of nasal clearance in man, monkey and other mammals. *Archiv Otolaryngol* 20(4):518–541
 96. Gray J (1930) The mechanism of ciliary movement—VI Photographic and stroboscopic analysis of ciliary movement. *P R Soc Lond B-Conta* 107(751):313–332. doi:[10.1098/Rspb.1930.0075](https://doi.org/10.1098/Rspb.1930.0075)
 97. Lierle DM, Moore PM (1934) Effects of drugs on ciliary activity of mucosa of upper respiratory tract. *Archiv Otolaryngol* 19(1):55–65
 98. Dalhamn T (1955) A method for determination in vivo of the rate of ciliary beat and mucous flow in the trachea. *Acta Physiol Scand* 33(1):1–5. doi:[10.1111/j.1748-1716.1955.tb01187.x](https://doi.org/10.1111/j.1748-1716.1955.tb01187.x)
 99. Blair A, Woods A (1969) The effects of isoprenaline, atropine and disodium cromoglycate on ciliary motility and mucous flow measured in vivo in cat. *Br J Pharmacol* 35(2):P379
 100. Carson S, Goldhamer R, Carpenter R (1966) Responses of ciliated epithelium to irritants. Mucus transport in the respiratory tract. *Am Rev Respir Dis* 93 (3):Suppl:86–92
 101. Hilding AC (1956) On cigarette smoking, bronchial carcinoma and ciliary action. II. Experimental study on the filtering action of cow's lungs, the deposition of tar in the bronchial tree and removal by ciliary action. *N Engl J Med* 254(25):1155–1160. doi:[10.1056/NEJM195606212542502](https://doi.org/10.1056/NEJM195606212542502)
 102. Sackner MA, Rosen MJ, Wanner A (1973) Estimation of tracheal mucous velocity by bronchofiberscopy. *J Appl Physiol* 34(4):495–499
 103. Svartengren K, Wiman LG, Thyberg P, Rigler R (1989) Laser light scattering spectroscopy: a new method to measure tracheobronchial mucociliary activity. *Thorax* 44(7):539–547
 104. Annis P, Landa J, Lichtiger M (1976) Effects of atropine on velocity of tracheal mucus in anesthetized patients. *Anesthesiology* 44(1):74–77
 105. Wanner A, Hirsch JA, Greenelth DE, Swenson EW, Fore T (1973) Tracheal mucous velocity in beagles after chronic exposure to cigarette smoke. *Arch Environ Health* 27(6):370–371
 106. Toomes H, Vogt-Moykopf I, Heller W, Ostertag H (1981) Measurement of mucociliary clearance in smokers and non-smokers using a bronchoscopic video-technical method. *Lung* 159(1):27–34
 107. Velasquez DJ, Morrow PE (1984) Estimation of guinea pig tracheobronchial transport rates using a compartmental model. *Exp Lung Res* 7(3–4):163–176

108. Bermbach S, Weinhold K, Roeder T, Petersen F, Kugler C, Goldmann T, Rupp J, König P (2014) Mechanisms of cilia-driven transport in the airways in the absence of mucus. *Am J Respir Cell Mol Biol*. doi:[10.1165/rcmb.2012-0530OC](https://doi.org/10.1165/rcmb.2012-0530OC)
109. Spungin B, Silberberg A (1984) Stimulation of mucus secretion, ciliary activity, and transport in frog palate epithelium. *Am J Physiol* 247(5 Pt 1):C299–C308
110. Gatto LA (1993) Cholinergic and adrenergic stimulation of mucociliary transport in the rat trachea. *Respir Physiol* 92(2):209–217
111. König P, Krain B, Krasteva G, Kummer W (2009) Serotonin increases cilia-driven particle transport via an acetylcholine-independent pathway in the mouse trachea. *Plos One* 4(3):e4938. doi:[10.1371/journal.pone.0004938](https://doi.org/10.1371/journal.pone.0004938)
112. Klein MK, Haberberger RV, Hartmann P, Faulhammer P, Lips KS, Krain B, Wess J, Kummer W, König P (2009) Muscarinic receptor subtypes in cilia-driven transport and airway epithelial development. *Eur Respir J* 33(5):1113–1121. doi:[10.1183/09031936.00015108](https://doi.org/10.1183/09031936.00015108)
113. Fliegau M, Sonnen AF, Kremer B, Henneke P (2013) Mucociliary clearance defects in a murine in vitro model of pneumococcal airway infection. *PLoS One* 8(3):e59925. doi:[10.1371/journal.pone.0059925](https://doi.org/10.1371/journal.pone.0059925)
114. Ryser M, Burn A, Wessel T, Frenz M, Ricka J (2007) Functional imaging of mucociliary phenomena. *Eur Biophys J Biophys* 37(1):35–54. doi:[10.1007/S00249-007-0153-3](https://doi.org/10.1007/S00249-007-0153-3)
115. Jonas S, Zhou E, Deniz E, Huang B, Chandrasekera K, Bhat-tacharya D, Wu Y, Fan R, Deserno TM, Khokha MK, Choma MA (2013) A novel approach to quantifying ciliary physiology: microfluidic mixing driven by a ciliated biological surface. *Lab Chip* 13(21):4160–4163. doi:[10.1039/C3lc50571e](https://doi.org/10.1039/C3lc50571e)
116. Boling JL, Blandau RJ (1971) Egg transport through ampullae of oviducts of rabbits under various experimental conditions. *Biol Reprod* 4(2):174–184
117. Harper MJ (1961) Mechanisms involved in movement of newly ovulated eggs through ampulla of rabbit fallopian tube. *J Reprod Fertil* 2(4):522
118. Avendano S, Pelaez J, Croxatto HB (1971) Transport of microspheres by human oviduct in-vitro and effect of treatment with megestrol acetate. *J Reprod Fertil* 27(2):261–264
119. Gaddum-Rosse P, Blandau RJ, Thiersch JB (1973) Ciliary activity in the human and *Macaca nemestrina* oviduct. *Am J Anat* 138(2):269–275. doi:[10.1002/aja.1001380210](https://doi.org/10.1002/aja.1001380210)
120. Halbert SA, Becker DR, Szal SE (1989) Ovum transport in the rat oviductal ampulla in the absence of muscle contractility. *Biol Reprod* 40(6):1131–1136
121. Halbert SA, Tam PY, Blandau RJ (1976) Egg transport in the rabbit oviduct: the roles of cilia and muscle. *Science* 191(4231):1052–1053
122. Borell U, Nilsson O, Westman A (1957) Ciliary activity in the rabbit fallopian tube during oestrus and after copulation. *Acta Obstet Gynecol Scand* 36(1):22–28
123. Paton DM, Widdicombe JH, Rheaume DE, Johns A (1977) The role of the adrenergic innervation of the oviduct in the regulation of mammalian ovum transport. *Pharmacol Rev* 29(2):67–102
124. Kolle S, Dubielzig S, Reese S, Wehrend A, König P, Kummer W (2009) Ciliary transport, gamete interaction, and effects of the early embryo in the oviduct: ex vivo analyses using a new digital videomicroscopic system in the cow. *Biol Reprod* 81(2):267–274. doi:[10.1095/biolreprod.108.073874](https://doi.org/10.1095/biolreprod.108.073874)
125. Shi D, Komatsu K, Uemura T, Fujimori T (2011) Analysis of ciliary beat frequency and ovum transport ability in the mouse oviduct. *Genes Cells* 16(3):282–290. doi:[10.1111/j.1365-2443.2011.01484.x](https://doi.org/10.1111/j.1365-2443.2011.01484.x)
126. Kolle S (2012) Live Cell Imaging of the Oviduct. Imaging and spectroscopic analysis of living cells: imaging live cells in health and disease 506:415–423. doi:[10.1016/B978-0-12-391856-7.00045-7](https://doi.org/10.1016/B978-0-12-391856-7.00045-7)
127. Nonaka S, Yoshida S, Watanabe D, Ikeuchi S, Goto T, Marshall WF, Hamada H (2005) De novo formation of left–right asymmetry by posterior tilt of nodal cilia. *PLoS Biol* 3(8):1467–1472. doi:[10.1371/journal.pbio.0030268](https://doi.org/10.1371/journal.pbio.0030268)
128. Inoué S (2006) Foundations of confocal scanned imaging in light microscopy. In: Pawley JB (ed) *Handbook of biological confocal microscopy*, 3rd edn. Springer, New York, p xxviii, p 985
129. Winet H, Yates GT, Wu TY, Head J (1982) On the mechanics of mucociliary flows. II. A fluorescent tracer method for obtaining flow velocity profiles in mucus. *Prog Clin Biol Res* 80:29–34
130. Cheng P-C (2006) The contrast formation in optical microscopy. In: Pawley JB (ed) *Handbook of biological confocal microscopy*, 3rd edn. Springer, New York, p xxviii, p 985
131. Winet H, Yates GT, Wu TY, Head J (1984) On the mechanics of mucociliary flows. III. Flow-velocity profiles in frog palate mucus. *J Appl Physiol Respir Environ Exerc Physiol* 56(3):785–794
132. Deblandre GA, Wettstein DA, Koyano-Nakagawa N, Kintner C (1999) A two-step mechanism generates the spacing pattern of the ciliated cells in the skin of *Xenopus* embryos. *Development* 126(21):4715–4728
133. Mitchell B, Stubbs JL, Huisman F, Taborek P, Yu C, Kintner C (2009) The PCP pathway instructs the planar orientation of ciliated cells in the *Xenopus* larval skin. *Curr Biol* 19(11):924–929. doi:[10.1016/J.Cub.04.018](https://doi.org/10.1016/J.Cub.04.018)
134. Zeltner TB, Sweeney TD, Skornik WA, Feldman HA, Brain JD (1991) Retention and clearance of 0.9-micron particles inhaled by hamsters during rest or exercise. *J Appl Physiol* 70(3):1137–1145
135. Francis RJ, Chatterjee B, Loges NT, Zentgraf H, Omran H, Lo CW (2009) Initiation and maturation of cilia-generated flow in newborn and postnatal mouse airway. *Am J Physiol Lung Cell Mol Physiol* 296(6):L1067–L1075. doi:[10.1152/ajplung.00001.2009](https://doi.org/10.1152/ajplung.00001.2009)
136. Tarran R, Boucher RC (2002) Thin-film measurements of airway surface liquid volume/composition and mucus transport rates in vitro. *Methods Mol Med* 70:479–492. doi:[10.1385/1-59259-187-6:479](https://doi.org/10.1385/1-59259-187-6:479)
137. Matsui H, Grubb BR, Tarran R, Randell SH, Gatzky JT, Davis CW, Boucher RC (1998) Evidence for periciliary liquid layer depletion, not abnormal ion composition, in the pathogenesis of cystic fibrosis airways disease. *Cell* 95(7):1005–1015
138. Worthington E, Tarran R (2011) Methods for ASL measurements and mucus transport rates in cell cultures. In: Amaral MD, Kunzelmann K (eds) *Cystic Fibrosis*, vol 742. *Methods in Molecular Biology*. Humana Press, pp 77–92. doi:[10.1007/978-1-61779-120-8_5](https://doi.org/10.1007/978-1-61779-120-8_5)
139. Hussong J, Lindken R, Faulhammer P, Noreikat K, Sharp KV, Kummer W, Westerweel J (2013) Cilia-driven particle and fluid transport over mucus-free mice tracheae. *J Biomech* 46(3):593–598. doi:[10.1016/J.jbiomech.2012.08.020](https://doi.org/10.1016/J.jbiomech.2012.08.020)
140. Satir P, Christensen ST (2007) Overview of structure and function of mammalian cilia. *Annu Rev Physiol* 69:377–400. doi:[10.1146/annurev.physiol.69.040705.141236](https://doi.org/10.1146/annurev.physiol.69.040705.141236)
141. Nonaka S (2013) Visualization of mouse nodal cilia and nodal flow. *Method Enzymol* 525:149–157. doi:[10.1016/B978-0-12-397944-5.00008-0](https://doi.org/10.1016/B978-0-12-397944-5.00008-0)
142. Takeda S, Yonekawa Y, Tanaka Y, Okada Y, Nonaka S, Hirokawa N (1999) Left-right asymmetry and kinesin superfamily protein KIF3A: new insights in determination of laterality and mesoderm induction by kif3A–/– mice analysis. *J Cell Biol* 145(4):825–836
143. Nonaka S, Tanaka Y, Okada Y, Takeda S, Harada A, Kanai Y, Kido M, Hirokawa N (1998) Randomization of left-right

- asymmetry due to loss of nodal cilia generating leftward flow of extraembryonic fluid in mice lacking KIF3B motor protein. *Cell* 95(6):829–837. doi:[10.1016/S0092-8674\(00\)81705-5](https://doi.org/10.1016/S0092-8674(00)81705-5)
144. Vick P, Schweickert A, Weber T, Eberhardt M, Mencl S, Scherbakov D, Beyer T, Blum M (2009) Flow on the right side of the gastrocoel roof plate is dispensable for symmetry breakage in the frog *Xenopus laevis*. *Dev Biol* 331(2):281–291. doi:[10.1016/j.ydbio.2009.05.547](https://doi.org/10.1016/j.ydbio.2009.05.547)
 145. Yoshihara S, Shiratori H, Kuo IY, Kawasumi A, Shinohara K, Nonaka S, Asai Y, Sasaki G, Belo JA, Sasaki H, Nakai J, Dworniczak B, Ehrlich BE, Pennekamp P, Hamada H (2012) Cilia at the node of mouse embryos sense fluid flow for left-right determination via Pkd2. *Science* 338(6104):226–231. doi:[10.1126/Science.1222538](https://doi.org/10.1126/Science.1222538)
 146. Kramer-Zucker AG, Olale F, Haycraft CJ, Yoder BK, Schier AF, Drummond IA (2005) Cilia-driven fluid flow in the zebrafish pronephros, brain and Kupffer's vesicle is required for normal organogenesis. *Development* 132(8):1907–1921. doi:[10.1242/dev.01772](https://doi.org/10.1242/dev.01772)
 147. Essner JJ, Amack JD, Nyholm MK, Harris EB, Yost J (2005) Kupffer's vesicle is a ciliated organ of asymmetry in the zebrafish embryo that initiates left-right development of the brain, heart and gut. *Development* 132(6):1247–1260. doi:[10.1242/Dev.01663](https://doi.org/10.1242/Dev.01663)
 148. Nonaka S, Shiratori H, Saijoh Y, Hamada H (2002) Determination of left-right patterning of the mouse embryo by artificial nodal flow. *Nature* 418(6893):96–99. doi:[10.1038/Nature00849](https://doi.org/10.1038/Nature00849)
 149. Yamadori T, Nara K (1979) The directions of ciliary beat on the wall of the lateral ventricle and the currents of the cerebrospinal fluid in the brain ventricles. *Scan Electron Microsc* 3:335–340
 150. Del Bigio MR (1995) The ependyma: a protective barrier between brain and cerebrospinal fluid. *Glia* 14(1):1–13. doi:[10.1002/glia.440140102](https://doi.org/10.1002/glia.440140102)
 151. Cifuentes M, Rodriguez S, Perez J, Grondona JM, Rodriguez EM, Fernandezllebrez P (1994) Decreased cerebrospinal-fluid flow-through the central canal of the spinal-cord of rats immunologically deprived of reissners fiber. *Exp Brain Res* 98(3):431–440
 152. Taulman PD, Haycraft CJ, Balkovetz DF, Yoder BK (2001) Polaris, a protein involved in left-right axis patterning, localizes to basal bodies and cilia. *Mol Biol Cell* 12(3):589–599
 153. Sapiro R, Kostetskii I, Olds-Clarke P, Gerton GL, Radice GL, Strauss IJ (2002) Male infertility, impaired sperm motility, and hydrocephalus in mice deficient in sperm-associated antigen 6. *Mol Cell Biol* 22(17):6298–6305
 154. Ibanez-Tallon I, Pagenstecher A, Fliegauf M, Olbrich H, Kispert A, Ketelsen UP, North A, Heintz N, Omran H (2004) Dysfunction of axonemal dynein heavy chain Mdnah5 inhibits ependymal flow and reveals a novel mechanism for hydrocephalus formation. *Hum Mol Genet* 13(18):2133–2141. doi:[10.1093/hmg/ddh219](https://doi.org/10.1093/hmg/ddh219)
 155. Banizs B, Pike MM, Millican CL, Ferguson WB, Komlosi P, Sheetz J, Bell PD, Schwiebert EM, Yoder BK (2005) Dysfunctional cilia lead to altered ependyma and choroid plexus function, and result in the formation of hydrocephalus. *Development* 132(23):5329–5339. doi:[10.1242/Dev.022153](https://doi.org/10.1242/Dev.022153)
 156. Hagenlocher C, Walentek P, ML C, Thumberger T, Feistel K (2013) Ciliogenesis and cerebrospinal fluid flow in the developing *Xenopus* brain are regulated by foxj1. *Cilia* 2(1):12. doi:[10.1186/2046-2530-2-12](https://doi.org/10.1186/2046-2530-2-12)
 157. Guirao B, Meunier A, Mortaud S, Aguilar A, Corsi JM, Strehl L, Hirota Y, Desoeuvre A, Boutin C, Han YG, Mirzadeh Z, Cremer H, Montcouquiol M, Sawamoto K, Spassky N (2010) Coupling between hydrodynamic forces and planar cell polarity orients mammalian motile cilia. *Nat Cell Biol* 12(4):341–350. doi:[10.1038/ncb2040](https://doi.org/10.1038/ncb2040)
 158. Webb RH (1996) Confocal optical microscopy. *Rep Prog Phys* 59(3):427–471. doi:[10.1088/0034-4885/59/3/003](https://doi.org/10.1088/0034-4885/59/3/003)
 159. Jayaraman S, Song Y, Vetrivel L, Shankar L, Verkman AS (2001) Noninvasive in vivo fluorescence measurement of airway-surface liquid depth, salt concentration, and pH. *J Clin Invest* 107(3):317–324. doi:[10.1172/JCI11154](https://doi.org/10.1172/JCI11154)
 160. Tarran R, Grubb BR, Gatzky JT, Davis CW, Boucher RC (2001) The relative roles of passive surface forces and active ion transport in the modulation of airway surface liquid volume and composition. *J Gen Physiol* 118(2):223–236
 161. Tarran R, Trout L, Donaldson SH, Boucher RC (2006) Soluble mediators, not cilia, determine airway surface liquid volume in normal and cystic fibrosis superficial airway epithelia. *J Gen Physiol* 127(5):591–604. doi:[10.1085/Jgp.200509468](https://doi.org/10.1085/Jgp.200509468)
 162. Song Y, Namkung W, Nielson DW, Lee JW, Finkbeiner WE, Verkman AS (2009) Airway surface liquid depth measured in ex vivo fragments of pig and human trachea: dependence on Na⁺ and Cl⁻ channel function. *Am J Physiol Lung Cell Mol Physiol* 297(6):L1131–L1140. doi:[10.1152/ajplung.00085.2009](https://doi.org/10.1152/ajplung.00085.2009)
 163. Button B, Okada SF, Frederick CB, Thelin WR, Boucher RC (2013) Mechanosensitive ATP release maintains proper mucus hydration of airways. *Sci Signal* 6(279):ra46. doi:[10.1126/scisignal.2003755](https://doi.org/10.1126/scisignal.2003755)
 164. Voynow JA, Rubin BK (2009) Mucins, mucus, and sputum. *Chest* 135(2):505–512. doi:[10.1378/chest.08-0412](https://doi.org/10.1378/chest.08-0412)
 165. Button B, Cai LH, Ehre C, Kesimer M, Hill DB, Sheehan JK, Boucher RC, Rubinstein M (2012) A periciliary brush promotes the lung health by separating the mucus layer from airway epithelia. *Science* 337(6097):937–941. doi:[10.1126/science.1223012](https://doi.org/10.1126/science.1223012)
 166. Kiyota K, Ueno H, Numayama-Tsuruta K, Haga T, Imai Y, Yamaguchi T, Ishikawa T (2014) Fluctuation of cilia-generated flow on the surface of the tracheal lumen. *Am J Physiol Lung Cell Mol Physiol* 306(2):L144–L151. doi:[10.1152/ajplung.00117.2013](https://doi.org/10.1152/ajplung.00117.2013)
 167. Druart X, Cognie J, Baril G, Clement F, Dacheux JL, Gatti JL (2009) In vivo imaging of in situ motility of fresh and liquid stored ram spermatozoa in the ewe genital tract. *Reproduction* 138(1):45–53. doi:[10.1530/REP-09-0108](https://doi.org/10.1530/REP-09-0108)
 168. Kolle S, Reese S, Kummer W (2010) New aspects of gamete transport, fertilization, and embryonic development in the oviduct gained by means of live cell imaging. *Theriogenology* 73(6):786–795. doi:[10.1016/j.theriogenology.2009.11.002](https://doi.org/10.1016/j.theriogenology.2009.11.002)
 169. Supatto W, Fraser SE, Vermot J (2008) An all-optical approach for probing microscopic flows in living embryos. *Biophys J* 95(4):L29–L31. doi:[10.1529/Biophysj.108.137786](https://doi.org/10.1529/Biophysj.108.137786)
 170. Hadjantonakis AK, Pisano E, Papaioannou VE (2008) Tbx6 Regulates Left/Right Patterning in Mouse Embryos through Effects on Nodal Cilia and Perinodal Signaling. *Plos One* 3(6):e2511. doi:[10.1371/journal.pone.0002511](https://doi.org/10.1371/journal.pone.0002511)
 171. Hess ST, Webb WW (2002) Focal volume optics and experimental artifacts in confocal fluorescence correlation spectroscopy. *Biophys J* 83(4):2300–2317
 172. Derichs N, Jin BJ, Song Y, Finkbeiner WE, Verkman AS (2011) Hyperviscous airway periciliary and mucous liquid layers in cystic fibrosis measured by confocal fluorescence photobleaching. *FASEB J* 25(7):2325–2332. doi:[10.1096/fj.10-179549](https://doi.org/10.1096/fj.10-179549)
 173. Boukari H, Brichacek B, Stratton P, Mahoney SF, Lifson JD, Margolis L, Nossal R (2009) Movements of HIV-virions in human cervical mucus. *Biomacromolecules* 10(9):2482–2488. doi:[10.1021/bm900344q](https://doi.org/10.1021/bm900344q)
 174. Stelzer EHK (1995) The Intermediate Optical System of Laser-Scanning Confocal Microscopes. In: Pawley JB (ed) *Handbook of biological confocal microscopy*, 2nd edn. Plenum Press, New York, pp xxiii, 632 p., p 634 of plates

175. Callamaras N, Parker I (1999) Radial localization of inositol 1,4,5-trisphosphate-sensitive Ca^{2+} release sites in *Xenopus* oocytes resolved by axial confocal line scan imaging. *J Gen Physiol* 113(2):199–213. doi:[10.1085/Jgp.113.2.199](https://doi.org/10.1085/Jgp.113.2.199)
176. Huang D, Swanson EA, Lin CP, Schuman JS, Stinson WG, Chang W, Hee MR, Flotte T, Gregory K, Puliafito CA, Fujimoto JG (1991) Optical Coherence Tomography. *Science* 254(5035):1178–1181. doi:[10.1126/Science.1957169](https://doi.org/10.1126/Science.1957169)
177. Fercher AF, Drexler W, Hitzenberger CK, Lasser T (2003) Optical coherence tomography—principles and applications. *Rep Prog Phys* 66(2):239–303. doi:[10.1088/0034-4885/66/2/204](https://doi.org/10.1088/0034-4885/66/2/204) (Pii S0034-4885(03)18703-9)
178. Wojtkowski M (2010) High-speed optical coherence tomography: basics and applications. *Appl Optics* 49(16):D30–D61. doi:[10.1364/Ao.49.000d30](https://doi.org/10.1364/Ao.49.000d30)
179. Jonas S, Bhattacharya D, Khokha MK, Choma MA (2011) Microfluidic characterization of cilia-driven fluid flow using optical coherence tomography-based particle tracking velocimetry. *Biomed Optics Express* 2(7):2022–2034. doi:[10.1364/BOE.2.002022](https://doi.org/10.1364/BOE.2.002022)
180. Oldenburg AL, Chhetri RK, Hill DB, Button B (2012) Monitoring airway mucus flow and ciliary activity with optical coherence tomography. *Biomed Optics Express* 3(9):1978–1992. doi:[10.1364/BOE.3.001978](https://doi.org/10.1364/BOE.3.001978)
181. Leitgeb RA, Villiger M, Bachmann AH, Steinmann L, Lasser T (2006) Extended focus depth for Fourier domain optical coherence microscopy. *Opt Lett* 31(16):2450–2452. doi:[10.1364/Ol.31.002450](https://doi.org/10.1364/Ol.31.002450)
182. Liu L, Gardecki JA, Nadkarni SK, Toussaint JD, Yagi Y, Bouma BE, Tearney GJ (2011) Imaging the subcellular structure of human coronary atherosclerosis using micro-optical coherence tomography. *Nat Med* 17(8):1010–1014. doi:[10.1038/nm.2409](https://doi.org/10.1038/nm.2409)
183. Liu LB, Chu KK, Houser GH, Diephuis BJ, Li Y, Wilsterman EJ, Shastry S, Dierksen G, Birket SE, Mazur M, Byan-Parker S, Grizzle WE, Sorscher EJ, Rowe SM, Tearney GJ (2013) Method for quantitative study of airway functional microanatomy using micro-optical coherence tomography. *Plos One* 8(1):e54473. doi:[10.1371/journal.pone.0054473](https://doi.org/10.1371/journal.pone.0054473)
184. Liu L, Shastry S, Byan-Parker S, Houser G, Chu K, Birket SE, Fernandez CM, Gardecki JA, Grizzle W, Wilsterman EJ, Sorscher EJ, Rowe SM, Tearney GJ (2014) An autoregulatory mechanism governing mucociliary transport is sensitive to mucus load. *Am J Respir Cell Mol Biol*. doi:[10.1165/rmb.2013-0499MA](https://doi.org/10.1165/rmb.2013-0499MA)
185. Chhetri RK, Kozek KA, Johnston-Peck AC, Tracy JB, Oldenburg AL (2011) Imaging three-dimensional rotational diffusion of plasmon resonant gold nanorods using polarization-sensitive optical coherence tomography. *Phys Rev E Stat Nonlin Soft Matter Phys* 83(4 Pt 1):040903
186. Patil CA, Bosschaart N, Keller MD, van Leeuwen TG, Mahadevan-Jansen A (2008) Combined Raman spectroscopy and optical coherence tomography device for tissue characterization. *Opt Lett* 33(10):1135–1137
187. Weers J, Metzheiser B, Taylor G, Warren S, Meers P, Perkins WR (2009) A gamma scintigraphy study to investigate lung deposition and clearance of inhaled amikacin-loaded liposomes in healthy male volunteers. *J Aerosol Med Pulm Drug Deliv* 22(2):131–138
188. Negus VE (1934) Action of cilia and the effect of drugs on their activity. Wellcome Library, UK